EVOLUTION OF LIESEGANG PATTERNS THROUGH GEL CONCENTRATION BORDERS AND THERMAL CHANGES

A THESIS SUBMITTED TO

THE GRADUATE SCHOOL OF ENGINEERING AND

SCIENCE

OF BILKENT UNIVERSITY

IN PARTIAL FULLFILMENT OF THE REQUIREMENTS

FOR

THE DEGREE OF

MASTER OF SCIENCE

IN CHEMISTRY

BY

ELİF SILA AKBULUT

AUGUST 2023

EVOLUTION OF LIESEGANG PATTERNS THROUGH GEL CONCENTRATION BORDERS AND THERMAL CHANGES

By Elif Sıla Akbulut

August 2023

We certify that we have read thesis and that in our opinion it is fully adequate, in scope and in quality, as a thesis for the degree of Master of Science.

_____

Bilge BAYTEKIN (Advisor)

_____

Ferdi KARADAŞ

_____

István LAGZI

Approved for the Graduate School of Engineering and Science:

_____

Orhan ARIKAN

Director of the Graduate School

ABSTRACT

Evolution of Liesegang Patterns Through Gel Concentration

Borders and Thermal Changes

Elif Sıla Akbulut

M.S in Chemistry

Advisor: Bilge BAYTEKIN

August 2023

Liesegang Patterns (LPs) are under the umbrella of periodic precipitation patterns that are formed through reaction- diffusion (RD). Liesegang Patterns can be used to track down the changes in the physical environment, because different physical environments produce different environments. Since their discovery effects of various parameters such as temperature, magnetic ,and electric fields, concentrations of electrolytes and gels have been studied to understand the formation mechanisms of these patterns. In this study an LP system ($CuSO_4$ (outer electrolyte)/ K_2CrO_4 (inner electrolyte) in agarose hydrogel) that responds to changes in the gel environments was generated. The medium uniformity with different gel concentration regions designed in various geometries (circle, square, triangle, and pentagon) were used to break the symmetry ,and homogeneity in the medium. The propagation of LP waves across the boundaries between the regions was visually inspected. The LP band spacings, the size ,and morphology of the product within the bands were altered in comparison to those observed in with LPs in homogenous media. The first part of the work is the first display of LP waves travelling through concentration boundaries. The visual patterns obtained in spatially heterogeneous media provide complex patterning of matter, which is not only fundamentally interesting for the study of artificial patterning but also can be useful in fields such as catalysis, and soft functional materials.

Second, the propagation of the “bio” waves of bacteria colony *Bacillus Subtilis* growth through different concentration gel media was monitored. Different concentrations of agar ,and tryptone across a boundary in the growing medium led

to changes in the growth patterns of bacteria upon passing to the “other side”. These changes growing bacterial patterns can be used to analyse how the spatial changes in the environment affect the growing colonies ,and give a more realistic view on the bacterial growth on complex terrain.

Finally, we explore the effect of temperature ,and the hydrogel chemistry (gelatin, agarose, and PVA) on the formation of $Mg(OH)_2$ LPs. Previously, temperature was used only to change the LP spacings and particle size. This work shows that it can also be used to alter the morphology of the formed particles. The results of this part of the project imply that a temperature gradient can be used to produce patterns with diverse morphologies of the same species in the same spatial environment.

All these parts in the thesis work point out that simple symmetry breaking in the medium can make significant changes in the ‘developing’ systems in the macro, and micro scales. This information can be used in analysis ,and utilization of natural ,and synthetic patterns systems.

Keywords. Liesegang patterns, periodic precipitation, bacteria morphology, agarose hydrogel, particle growth

ÖZET

Jel Konsantrasyon Sınırları ve Termal Değişiklikler Yoluyla Liesegang Desenlerinin Evrimi

Elif Sıla Akbulut

Kimya, Yüksek Lisans

Tez Danışmanı : Bilge BAYTEKIN

Ağustos 2023

Liesegang Desenleri (LD'leri), reaksiyon-difüzyon (RD) yoluyla oluşan periyodik paternleri çatısı altındadır. LD'ler, fiziksel ortamdaki değişiklikleri izlemek için kullanılabilir, çünkü farklı fiziksel ortamlar farklı ortamlar üretir. Keşfedilmelerinden bu yana, sıcaklık, manyetik ve elektrik alanlar, elektrolit ve jel konsantrasyonları gibi çeşitli parametrelerin etkileri, bu desenlerin oluşum mekanizmalarını anlamak için incelenmiştir. Bu çalışmada jel ortamlarındaki değişikliklere tepki veren bir sistem (agaroz hidrojelde $CuSO_4$ (dış elektrolit)/ K_2CrO_4 (iç elektrolit)) oluşturuldu. Burada, çeşitli geometrilerde (daire, kare, üçgen ve beşgen) tasarlanmış farklı jel konsantrasyon bölgeleriyle uzamsal homojenlik bozularak LD dalgalarının bölgeler arasındaki sınırlar boyunca yayılması incelenmiştir.

Ortamdaki simetri ve homojenliği kırmak için çeşitli geometrilerde (daire, kare, üçgen ve beşgen) tasarlanmış farklı jel derişim bölgelerine sahip ortam homojenliği kullanılmıştır. LP dalgalarının bölgeler arasındaki sınırlar boyunca yayılması görsel olarak incelendi. LP bant aralıkları, bantlar içindeki ürünün boyutu ve morfolojisi, homojen ortamda LP'lerde gözlenenlere kıyasla değiştirildi. Çalışmanın ilk kısmı, derişim sınırlarından geçen LP dalgalarının ilk gösterimidir. Mekânsal olarak heterojen ortamlarda elde edilen görsel modeller, maddenin karmaşık modellenmesini sağlar; bu, yalnızca yapay modelleme çalışması için temelde ilginç olmakla kalmaz, aynı zamanda kataliz ve yumuşak fonksiyonel malzeme araştırmalar için de yararlıdır.

İkinci olarak, bakteri kolonisi Bacillus Subtilis'in "biyo" dalgalarının farklı konsantrasyondaki jel ortamları yoluyla yayılması izlendi. Büyüyen besiyerindeki bir sınır boyunca farklı agar ve tripton derişimleri, "diğer tarafa" geçtikten sonra bakterilerin büyüme modellerinde değişikliklere yol açmıştır. Büyüyen bakteri kalıplarındaki bu değişiklikler, ortamdaki mekânsal değişikliklerin büyüyen kolonileri nasıl etkilediğini analiz etmek ve karmaşık arazide bakteri büyümesi hakkında daha gerçekçi bir görünüm vermek için kullanılabilir.

Son olarak, sıcaklığın ve hidrojel kimyasının (jelatin, agaroz ve PVA) $Mg(OH)_2$ LD'lerin oluşumu üzerindeki etkisini araştırılmıştır. Önceden, sıcaklık yalnızca LP aralıklarını ve parçacık boyutunu değiştirmek için kullanılmıştır. Bu çalışma, parçacıkların morfolojisini değiştirmek için de kullanılabileceğini göstermektedir. Projenin bu bölümünün sonuçları, sıcaklık gradyanının aynı uzaysal ortamda aynı türün farklı morfolojik parçacıklarını birlikte üretmek ve modellemek için kullanılabileceğini göstermektedir.

Tez çalışmasındaki tüm bu kısımlar, ortamdaki basit simetri kırılmalarının makro ve mikro ölçekte 'gelişmekte olan' sistemlerde önemli değişiklikler yapabileceğine işaret etmektedir. Bu bilgi, doğal ve sentetik model sistemlerinin analizinde ve kullanımında kullanılabilir.

Anahtar Kelimeler. Liesegang Desenleri, periodik çökelme, bakteri morfolojisi, agaroz hidrojel ve parçacık büyümesi

ACKNOWLEDGMENTS

I would like to thank my advisor, Dr. Bilge Baytekin for her endless support, motivation videos, breathing exercises, being a source of inspiration, and a wall for me to always feel the support of. I would like to thank Dr. Istvan Lagzi and Dr. Ferdi Karadaş for being in my thesis committee, and providing feedbacks to improve my thesis.

I would like to thank my greatest supporters, my family… My father, mother, sister, my niece, and my cats: Sinba, Coco, Pıtırcık, Petek, Bıcır, and Pakize… Thank you for always being present with me at the sleepless nights, nervous breakdowns. I would not be me, without you.

I am grateful for my best friends Gökçe Dilek, Yağmur Censur, Ecem Uzun Bengisu Seçkin, and Güliz Başak Özkan, thank you for being my northern stars ,and eliminating my path.

This thesis would not be complete without my lovely tripods Elvan Gören, Eylül Ergün, and Nurbanu Çakır. Thank you for helping with my experiments, taking pictures, and not leaving me when I was too much to be around. I want to thank Ekin Bircan Boşdurmaz, for all the time we spent looking for particles with SEM.

I would like to thank my dear friends from the Baytekin Research Group, Sunay Dilara Ekim and Levent Bahçeci, the long hours in the lab would not be as enjoyable without you. However, above all I am grateful for Rana Uzunlar and Merve Temel (the honorary Baytekin Research Group Member), thank you for being my baseline of reason and a shoulder for me to cry on. Here I also want to mention two more friends I met at Bilkent and intending to keep for life; Eylül Çalıkyılmaz and Bilge Banu Yağcı. Thank you for all the coffee, advice, and mostly for your friendship.

I would like to thank Prof. Dr. Urartu Şeker and Cem Polat, for their help in bacteria studies. I acknowledge TÜBİTAK for providing financial support under the project no: 219Z263

Table of Contents

List of Figures

Figure 7. (a) SEM micrographs of ring 1 on agarose hydrogel from samples of different concentrations from 1.0 to 5.0 % w/v. (b) The histograms denoting the particle size distribution. The scale bar is 5 µm. The error bars are calculated from the standard deviations of the distribution.

Figure 8. (a) SEM micrographs of Ring 6 on agarose hydrogel from samples of different concentrations from 1.0 to 5.0 % w/v. (b) The histograms denoting the particle size distribution. The scale bar is 5 µm. The error bars are calculated from the standard deviations of the distribution.

Figure 9. Average $CuCrO_4$ particle size of (a) ring 1 ,and (b) ring 6 at different concentrations of agarose within the range of 1.0 to 5.0 % w/v. Error bars are calculated from the standard deviations of the distributions.

Figure 10. The increasing complexity of $CuCrO_4$ LPs forming in hydrogels. (*Centre to out*) (a) The LP formation in a homogeneous environment produces only regular LPs – concentric rings obeying spacing laws. (b) Patterns forming in heterogeneous fields lead to more complex LP patterns. Temperature change (low-high-low), or mechanical field change (stretch-release) were previously shown to yield deviations from the LP spacing rules. These deviations can be used to track back the environmental changes during LP formation. (c) A change in the concentration field with geometrical boundaries adds complexity to the patterns [42].

Figure 11. (a) The effect of polygon shape on the spacing coefficient in high ,and low concentration regions. (b) The spacing coefficients in the inner (5.0% w/v, blue) ,and outer (0.5% w/v, orange) regions of the polygons. LP patterns change their spacing coefficient entering the lower gel concentration region. The circular boundary region affects the greatest changes in the spacing coefficient. In all samples: $[K_2CrO_4]$ = 0.10 M (inner electrolyte) ,and $[CuSO_4]$ = 1.00 M (outer electrolyte), t = 3 days. Error bars denote the standard deviation from at least five independent measurements [42].

Figure 12. The effect of the physical boundary on the curvature of the produced LPs in the outer region (5.0 % w/v) (a) The **dotted** red lines denote the imaginary circles fitted to the first LP ring in the outer, less-concentrated region (b) The corresponding curvature values of the samples calculated by taking the reciprocal of the imaginary circle radii values in (a). [K_2CrO_4] = 0.10 M (inner electrolyte) ,and [$CuSO_4$] = 1.00 M (outer electrolyte), *t* = 3 days. Error bars denote the standard deviation from at least five independent measurements [42].

Figure 13. The LPs going through the concentration boundary can yield particles of different morphologies across the boundaries. (a) 1D $CuCrO_4$ LP system, (b-e) Scanning Electron Microscopy (SEM) micrographs of $CuCrO_4$ precipitates in LP bands in band 14 to band 17, respectively. The dashed red line denotes the boundary between the regions of different gel concentrations. The scale bar is 5 µm [42].

Figure 14. XRD diffractogram of copper (II) chromate particles developed on different concentrations of agarose 0.5 % w/v (orange), 1.0 % w/v (green) ,and 5.0 % w/v (navy) gel. The reference XRD diffractogram of $CuCrO_4$ is given in red [44].

Figure 15. The numerical simulations of the LP development through the high gel concentration to the low gel concentration regions. The red line in (a-d) is the boundary shape [42].

Figure 16. The refraction of the LP bands through a tilted boundary separating the high gel ,and low gel concentration regions in a 1D diffusion setup. (a) experimental result ,and (b) numerical simulation. The dotted red line denotes the boundary between the regions of 0.5 w/v ,and 5.0 w/v agarose. [K_2CrO_4] = 0.10 M (inner electrolyte) ,and [$CuSO_4$] = 1.0 M (outer electrolyte), pattern formation is tracked for 24 hours [42].

Figure 17. Schematic representation of the Snell's Law. v_1 ,and v_2 are the speeds of the waves in the respective media, θ_i is the incident angle ,and θ_t is the transmitted angle.

Figure 18. Common growth patterns of bacteria, (a) diffusion- Limited Aggregation (DLA), (b) dense- Branching Morphology (DBM), (c) concentric Ring Morphology (d) eden-like ring morphologies. Image is reproduced from [46].

Figure 19. Effect of agar ,and tryptone concentrations on the morphology of bacteria growth. Pattern formation is tracked for 7 days.

Figure 20. Bacteria growth evolution on different gel concentrations through a spherical boundary (a) 1.5 % w/v agar outside, (b) 2.0 % w/v agar outside, (b) (a-b) 1.0 % w/v agar inside , tryptone = 2.0 % w/v, (c) 1.5 % w/v agar outside (d) 2.0 % w/v agar outside (e) 2.5 % w/v agar outside (f) 3.0 % w/v agar outside (c-f) 1.0 % w/v agar inside , tryptone = 1.0 % w/v. The agar concentrations are denoted on the figure as well. Pattern formation is tracked for 7 days.

Figure 21. Bacteria growth evolution on different gel environments (a) 2.0 % w/v tryptone inside ,and 0.5 % w/v tryptone outside, agar is 2.0 % w/v for both regions (b) 1.0 % w/v tryptone inside ,and 0.5 % w/v tryptone outside, agar is 1.0 % w/v for both regions (c) 0.5 % w/v tryptone inside ,and 1.0 % w/v tryptone outside, agar concentration is 1.0 % w/v in both regions. The tryptone concentrations are denoted on the figure. Pattern formation is tracked for 7 days.

Figure 22. The effect of $MgSO_4$ concentration on the formation of $Mg(OH)_2$ LPs in gels without (left) ,and with (right) crosslinked 5.0 % w/v gelatin. The inner electrolyte concentration was altered from 0.40 M to 0.08 M. $[NH_4OH]$= 15 M. The pattern formation is tracked for 24 hours.

Figure 23. Formation of $Mg(OH)_2$ LPs on (a) agarose (b) gta-crosslinked gelatin ,and (c) gta-crosslinked PVA, in 24 hours. Pattern formation is tracked at 20^oC.

Figure 24. (a) Liesegang patterns formed at 10, 20, 30, 40 ^{o} C. Top to bottom: LPs developed in GTA-crosslinked gelatin, GTA-crosslinked PVA ,and agarose. The black line indicates the point of contact between the gel surface containing 0.10 M $MgSO_4$,and 15 M NH_4OH solution. (b) The variation of spacing coefficient in each of the samples at different temperatures. The error bars are calculated from the standard deviations of 5 samples. The pattern formation is tracked for 24 hours.

Figure 25. SEM micrographs of $Mg(OH)_2$ particles of different morphologies on GTA-crosslinked gelatin hydrogel. The scale bar is 10 µm except stated otherwise.

Figure 26. (a) SEM micrographs of band 1 on agarose hydrogel from samples at different temperatures 10-40 ^{o}C. (b) The histograms denoting the particle size distribution. The scale bar is 10 µm.

Figure 27. (a) SEM micrographs of band 2 on agarose hydrogel from samples at different temperatures 10-40 ^{o}C. (b) The histograms denoting the particle size distribution. The scale bar is 10 µm.

Figure 28. Average particle size in ring 1 (blue) , and in ring 2 (orange) on agarose hydrogel at 10-40 ^{o} C. The error bars are calculated from the standard deviations of the distributions.

Figure 29. (a) SEM micrographs of band 1 on crosslinked PVA with GTA hydrogel from samples at different temperatures 10- 40 ^{o}C. (b) The histograms denoting the particle size distribution. The scale bar is 10 µm.

Figure 30. (a) SEM micrographs of band 2 on glutaraldehyde-crosslinked PVA hydrogel from samples at different temperatures 10- 40 ^{o}C. (b) The histograms denoting the particle size distribution. The scale bar is 10 µm.

Figure 31. Average particle size in (a) in ring 1 , and (b) in ring 2 on PVA hydrogel at different temperatures**.** The error bars are calculated from the standard deviations of the distributions.

Figure 32. The X-ray diffractograms of $Mg(OH)_2$ LPs on (a) agarose , and (b) gelatin. The reference XRD diffractogram of $Mg(OH)_2$ is given in red [56].

LIST OF TABLES

This thesis is dedicated to

Sinba, Coco, Pıtırcık, Petek,

Bıcır, and Pakize

Chapter I

I. Introduction:

As Alfred North Whitehead once said, “Art is the imposing of a pattern on experience ,and our aesthetic enjoyment is recognition of the pattern” ,and our duty as scientists is to understand the process behind the pattern formation [1]. Nature, the most skilled artist of all amazes us with beautiful ,and unorthodox patterns all over us. This amazement led us to mimic these patterns ,and understand the mechanisms behind the formation process [2].

There are many self-assembled pattern formations including Belousov-Zhabotinsky (BZ) waves [3], and Turing patterns [4] however the most overly recognized self- assembled pattern formation process is the Liesegang Patterns (LPs), discovered by Raphael L. Liesegang back in 1896.

He observed this phenomenon when he dropped a drop of silver (I) nitrate onto a gelatin layer containing aluminium dichromate ,and he observed formation of concentric layers of silver dichromate [5]. From this point any pattern displaying periodicity is classified as a Liesegang pattern. The literature is saturated with a wide variety of research regarding these mesmerizing patterns from both theoretical ,and experimental aspects. Since their discovery, multiple systems with various morphologies, to name a few revert-spaced [6], bands with secondary structures [7], spirals [8], fractals [9], and 3D helices [10] have been reported.

A typical Liesegang experiment is straightforward, one of the precipitating agents known as the inner electrolyte is mixed with the gel and later the other precipitation component known to be the outer electrolyte is poured from the top after the gel has set completely [11]. Typical reaction environments for formation of LPs are glass Pasteur pipettes for the 1D or in petri dish for the 2D LPs. Further Zhang et al. produced a 3D sphere of gelatin and they produced $CaHPO_4$ LPs [12]. While in the 1D experimental set-up the outer electrolyte solution is poured to the top of the column for the 2D set up, wet stamping method (WETS) is applied. Here a concentrated small agarose hydrogel (the stamp) is dipped into the outer

electrolyte solution and after the saturation it is placed on the middle and the diffusion takes place radially from there [13]. Depending on the identity of the LPs, patterns can form in a span of days to several weeks. While both magnesium hydroxide , and copper (II) chromate LPs form in days, Farkas et al. reported the formation of LPs with gold nanoparticles on agarose in a month range [14].

Although at the first glance LPs appear to be an abstract system, they are present in various areas of research [15]. The Liesegang rings can be modelled by treating them like a cellular automaton by describing the system's reaction, diffusion, nucleation, and aggregation processes and taking into consideration of fluctuations on microscopic level [15].

Cooperative bacterial colony development is perhaps the most well-known pattern formation of living systems. Both *Bacillus Subtillis* and Proteus mirabilis are famous for producing well-defined concentric patterns [16] [17]. Depending on the concentrations of the medium (i.e., agar) ,and the nutrient various other morphologies can be obtained as well. Bacteria are not the only organism to produce similar pattens to LPs. Fungus Beaveria (B.) Caledonica forms concentric rings in the presence of copper oxalate hydrate or copper phosphate crystals [18]. When the rings are analysed, the ratio of the distances between the successive rings' approaches to a constant value, meaning that they obey to spacing law. There are reports on Liesegang ring like structures on cancerous breast cells as well [19].

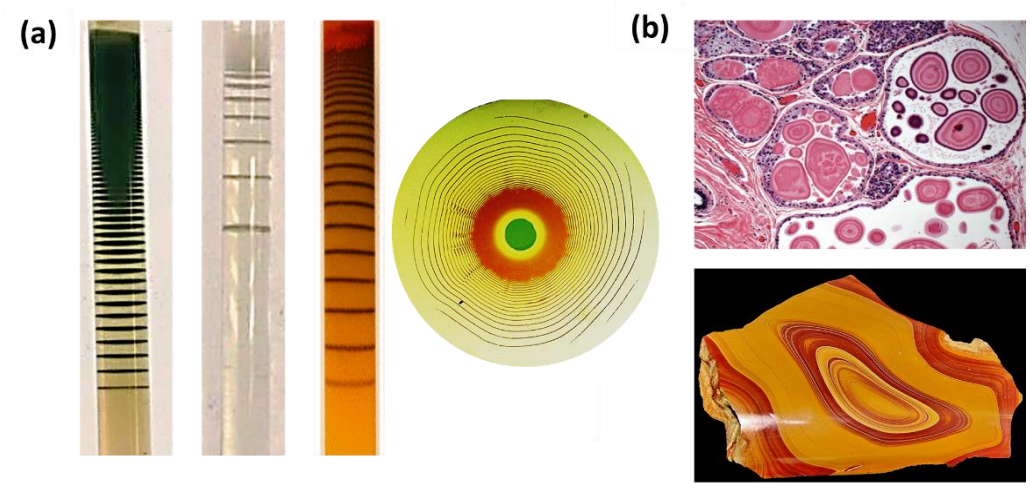

Figure 1. (a) Common Liesegang systems, from left to right $Co(OH)_2$, $Mg(OH)_2$, K_2CrO_4 ,and $CuCrO_4$. (b) Real-life examples to Liesegang patterns found in breast cancer cells , and in rocks. Images are reproduced from [19] [20].

Hydrogels are the gold standard medium to produce the LPs. Their popularity as a media comes from the fact that they prevent the convection of the formed precipitates and minimize the possible hydrodynamic effects due to convection [11]. LPs can also be produced in a wide variety of other media as well. The famous ring experiment of the freshman chemistry laboratory with HCl and NH_3 is an example to a gaseous LP system.

1.1 The Empirical Laws

There are three empirical laws governing the formation of the LPs; the spacing, time and width laws [21].

The Spacing law, which was first depicted by Jablczinsky in 1923, denotes the ratio between the distances of the adjacent rings is always constant thereby these patterns produce a geometric series [22]. Similarly, the width law forms a relation between the widths of the consecutive rings. Based on this law, the widths of the later rings are greater than the earlier rings.

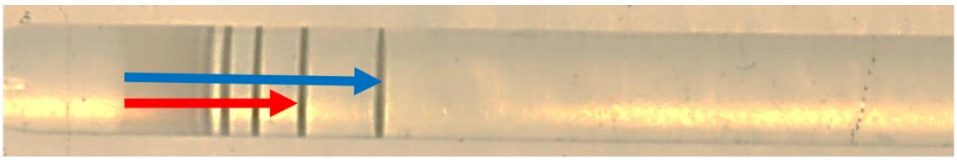

Spacing Law: $\frac{x_{n+1}}{x_n}$ Time Law: $x_n = \sqrt{t}$ Width Law: $\frac{w_{n+1}}{w_n}$

Figure 2. Mathematical relationships of spacing, time , and width laws of the Liesegang pattern are depicted. The x_{n+1} ,and x_n are the distances (positions) of (n+1) th ,and nth rings from the gel- outer electrolyte interface. The ratio of the positions of the consecutive bands yield to a constant, known as the p value. Similarly, w_{n+1} ,and w_n depict the widths of (n+1) th rings. The time law draws a relation between the position of a specific ring (x_n) ,and the time (t) it took for ring to appear.

The spacing coefficient (p) is utilized to understand the effects of the alterations in the external environment on the pattern formation. The relation between the electrolyte concentrations ,and the spacing coefficient is shown as the Matalon- Packter (MP) law [11] [23].

$$p = F(B_o) + G(B_o)\,\frac{B_o}{A_o}$$

Here A_0 and B_0 correspond to initial inner and outer electrolyte concentrations, F and G are monotonously decreasing functions of B_0. Based on this law, if we keep the outer electrolyte concentration constant ,and increase the inner electrolyte concentration, then the spacing coefficient (p) decrease.

Based on the spacing coefficient, we can subdivide LPs into two distinct categories, revert ,and direct types. In the direct type the spacing between the successive rings, in the revert type we observe a decrease in the spacing. While the log X_n versus n plot is a straight line for the direct type, the line deviates in the reverse type. Examples to direct type include $CuCrO_4$, Mg $(OH)_2$. LP system produced through the precipitation reaction of $AgNO_3$,and KBr is an example to a revert type LP system [24]. Other examples include $PbCrO_4$,and AgI LPs [25] [26].

1.2 Models to Understand the Formation of Liesegang Patterns

Although the Liesegang Patterns have been investigated more than a century still there is not a widely accepted mechanism explaining their formation. We can divide the approaches to explain the formation of Liesegang Patterns under two distinct categories, pre and post nucleation models.

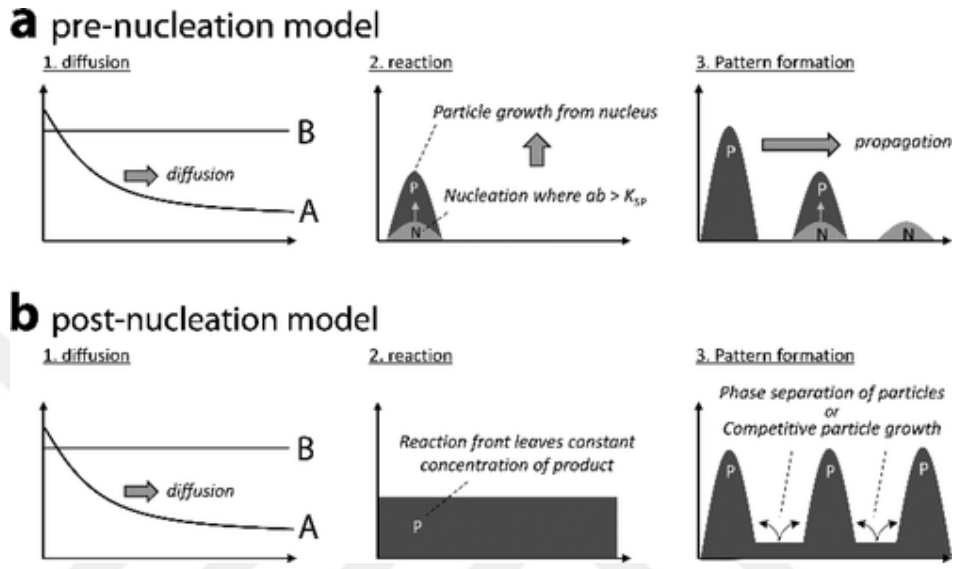

Figure 3. Differences between pre ,and post nucleation models of Liesegang band production. The image is reproduced from [11].

The Supersaturation Model

The first model to understand the formation of Liesegang Patterns was suggested by William Ostwald back in 1897. His idea is based on a simple precipitation reaction A (outer electrolyte) ,and B (inner electrolyte) to produce P (product).

$$A(aq) + B(aq) \longrightarrow P(s)$$

P only forms when the ion product AB exceeds the solubility product of the salt AB. The precipitate formation continues until the local product decreases. Once the precipitation occurs, we observe local depletion of reactant concentration and eventually the nucleation process stops. Once the local product of electrolytes concentrations reach the solubility product a new band forms. The continuous of this cycle, forms the periodic LPs. Although this model is consistent with the

empirical laws, it does not explain irregularities such as revert-spaced LPs, helices, and precipitates between the bands [11].

Nucleation- Growth Model

To overcome the existing problems of the previous theory, Nucleation - Growth Model has been proposed. According to this model, before the product formation an intermediate C forms ,and then it nucleates ,and grows to be P.

$$A(aq) + B(aq) \longrightarrow C(aq)$$

$$C(aq) \longrightarrow P(s)$$

Right at the hydrogel- outer electrolyte interface the supersaturation is so high that we observe immediate precipitation. With the formation of precipitate through nucleation and growth, the local concentration of the inner electrolyte decreases further from the precipitation zone ,and hence no new nucleation-growth occurs. Once the local products of electrolyte concentrations exceed the solubility product, we observe the formation of a new band. The repetition of this process produces the periodicity of the LPs.

Both the supersaturation and the nucleation - growth models are examples to prenucleation model.

The post nucleation model begins with the diffusion of the outer electrolyte to the gel. This leaves a constant concentration of particles. The bands form through phase separation and competitive particle growth. This model suggests that first the sol of the precipitate forms due to reaction of two electrolytes and disperses through the media. Later the LPs form through aggregation of later particles [27].

1.3 Effect of External Factors on the Formation of Liesegang Patterns

The Liesegang patterns are highly influenced by changes in the external environment including but not limited to electric and magnetic fields [28] [29] , temperature [30][31][32] , mechanical factors such as stretching ,and loading [33], gravity [34], light [35], concentrations of inner and outer electrolytes [36], pH [37], polarity of the solvent [38], and ionic strength [39].

In our previous endeavours with the LPs, we have investigated the effects of temperature on the production of $CuCrO_4$ LPs on polyacrylamide (PAM) hydrogel. Here the PAM hydrogel was chosen due to its high glass transition temperature which is above 150 ^oC . Since it is a chemically crosslinked hydrogel, it can stand to much higher temperatures compared to physically crosslinked cases such as gelatin ,and agarose. An increase in temperature leads both to an increase in the solubility product, K_{sp}, of $CuCrO_4$and the diffusion of copper chloride solution to the hydrogel. Once the temperature increases from 20 to 60 ^oC, the spacing coefficient of the system increases as demonstrated in Figure 4. Further temperature influences the morphology of the $CuCrO_4$ particles as well. An increase in temperature leads to an increase in the average particle size as well [30].

Temperature is the only factor that alters the reaction rates, diffusion, and precipitation thresholds singlehandedly thereby it is a significant parameter to produce LPs. Through our search of the literature, we came across a study investigating the relation of temperature ,and the production of magnesium hydroxide LPs on the agarose hydrogel within the temperature range of 25-43 ^oC [31]. Another study investigated temperature and the production of barium oxalate within a range of 31- 49 ^oC ,and while they observed an increase in the diffusion velocity ,and significant change in the spacing coefficient [32].

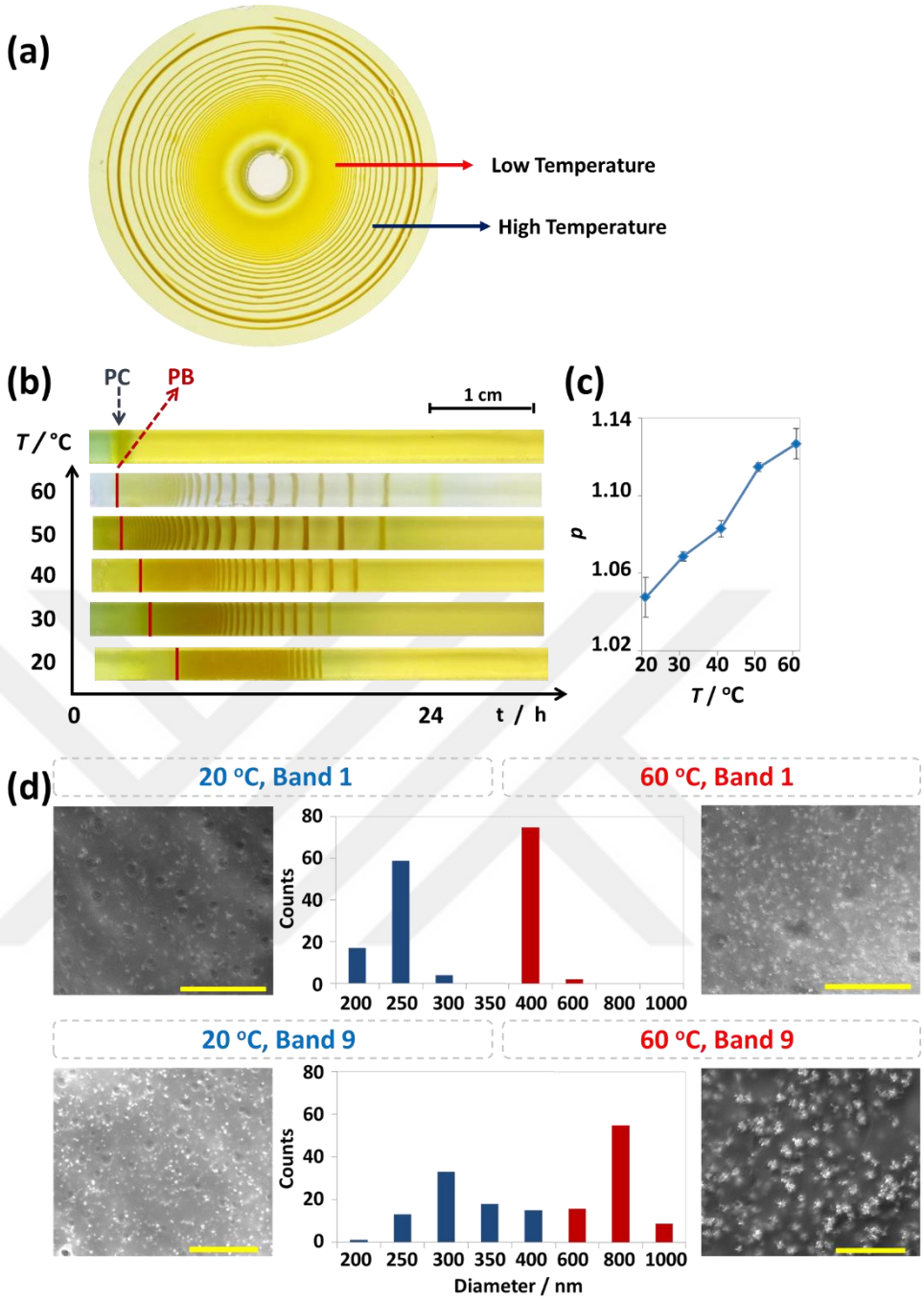

Figure 4. (a) LPs formed at low ,and high temperature regions. (b) Effect of temperature on the production of $CuCrO_4$ LPs on 1D array. (c) Change of p values with respect to temperature. (d) Effect of temperature on the average particle size of copper chromate at 20 ,and 60 ^{o}C, comparisons of bands 1 ,and 9. The system is composed of 1 M copper(II) chloride (outer electrolyte), 0.01 M potassium chromate (inner electrolyte) ,and polyacrylamide hydrogel (the medium). The image is reproduced from [29].

The aim of this thesis is to demonstrate the progress of Liesegang Patterns through change of media and mimic the natural patterns. This aim is conveyed through tracking the progress of Liesegang patterns through a change of concentration and temperature. We investigate how the pattern formation progresses on the regions with different concentrations using the example of $CuCrO_4$ LPs on agarose. We also assess the effect of chemical ,and temperature changes on the $Mg(OH)_2$ LP system at the macro and micro scale to test if this system is a useful candidate on spatial changes of these parameters. We expand 'the border' idea to the pattern formation on living media, through producing Bacillus Subtilis on Luria- Bertani (LB) medium with different concentrations of agar and tryptone.

Chapter II

II. Gel Lenses for Liesegang Waves

In this chapter we first describe the preparation of 2D $CuCrO_4$ LPs on agarose hydrogel at different concentrations. Then we investigated the effect of concentration of the medium on the spacing coefficient. Later by producing an artificial system, composed of low and high concentration media , we investigated how the presence of a boundary affects both the spacing coefficient of the system and the particle morphology. Our experimental results showed the similarities between our system and physical waves passing between regions of different refractive indices. Finally, we show the effect of a physical boundary on biological systems by analysing the growth patterns of *Bacillus Subtillis* on LB agar medium by altering the tryptone and agar concentrations.

2.1 Materials

Agarose (Fisher Bioreagents), copper (II) sulphate (AFG Bioscience), potassium chromate (Merck, 99.5 %), Agar (Serva), sodium chloride (Emsure®), yeast (Serva), tryptone from casein pancreatic (Serva)

Plexiglass and Parafilm® were used without any chemical modification.

2.2 The Experimental Method

2.2.1 Preparation of the Agarose Stamp

0.8 g of agarose was added to 10 ml of distilled water and this mixture was heated in a microwave until the agarose completely dissolved. Then the melted agarose was poured into a 3D-printed (Zortrax, M200) mold (for '2D', cylindrical: diameter = 1 cm, height = 0.8 cm; for '1D' cuboid: 1 cm × 1.5 cm × 1 cm). Samples in the molds were left for 30 minutes in a refrigerator and then the gellated stamps were soaked in 1.0 M of $CuSO_4$ outer electrolyte solutions overnight.

2.2.2 Preparation of Agarose Hydrogels with Added K_2CrO_4 Content

0.1 g of agarose ,and 0.04 g of potassium chromate were dissolved in 20 mL of distilled water to yield an 0.5% w/v agarose solution. The glass beaker was

covered with parafilm to avoid splashing and melting upon microwave heating. After the solution was obtained, the hydrogels were cast in Petri dishes with a diameter of 8.5 cm ,and were stored at room temperature for 3 hours for the complete gelation. The polygon shapes (triangle, square, pentagon, and hexagon) were cut from the centres of the samples. Then 0.5 g of agarose ,and 0.02 g of potassium chromate were dissolved in 10 mL of distilled water to yield a 5.0% w/v agarose solution. This solution was poured into the empty places in the samples, taking care that the height of the newly forming gel ,and the old gel were the same.

2.2.3 Optical Imaging

Images were captured using a Canon EOS Rebel T2i with a Canon EF 50 mm f/2.5 Macro Lens. Samples were illuminated from the bottom on a LED lightbox.

2.2.4 Image Processing and Analysis and the Determination of the Spacing Coefficient of the $CuCrO_4$ LPs

Data were extracted using ImageJ software. LP characterization was conducted using the Gray-value (pixel brightness, in the range of 0 to 225 in ImageJ software; gray-value = 0.229 × red + 0.587 × green + 0.114 × blue). Data collected using ImageJ was processed in MATLAB using a self-written MATLAB code exploiting the "Findpeaks" function to find the peaks' intensity, position, width, and *prominence* (the difference between the gray value of bands ,and their neighbour depletion zone). The spacing coefficient of the patterns signal ($x_{n+1}/x_n = 1 + p$) was retrieved from the slope of ln(x") vs. n, where x" ,and n are the position of the precipitation band ,and the band number, respectively, and ln(x")/n = ln (1 + p).

2.2.5 SEM and X-Ray Energy Dispersive Analysis of $CuCrO_4$ LPs

The LP-hydrogel samples were placed in glass flasks. Then the glass flasks were transferred to a liquid nitrogen bath for 10 minutes. The frozen hydrogels were cut in half with a steel blade ,and dried at vacuum for 24 hours.

The surface morphology of products was imaged with Quanta 200F model SEM with an accelerating voltage of 10 kV and spot size of 5. Samples were coated

with Au-Pd for imaging. The particle sizes were determined using the digital image analysis ImageJ software.

2.2.6 Preparation of Agar Plates

A solution of 0.5 g yeast ,and 1.0 g NaCl, 1.0 g tryptone as nutrient in 0.1 L of distilled water, adjusted at pH= 7.1 is mixed with 1.0 g of agar. Then the mixture is heated at 120 ^{o}C for 15 minutes ,and then poured into plastic petri dishes with a diameter of 90 mm (25 ml per plate). Then the plates are allowed to harden at room temperature for 1 hour. A circle with 40 mm diameter is cut from the middle, with a sterile petri dish ,and another solution of agar is poured down to cut shape. After allowing the system to fully dry, 5 µL of bacteria solution is placed onto the middle of the boundary. Samples are taken to the incubator at 30^{oo}, after the bacteria solution is fully dried. Pattern formation is tracked for 14 days.

For the preparation of plates, we changed the tryptone ,and agar concentrations within the ranges of (0.5, 1.0, 1.5, and 2.0) ,and (1.0, 1.5, 2.0, 2.5, and 3.0) respectively.

2.2.7 Incubation

The strain was inoculated on the plate surface at the centre of the agar plate. Plates were stored at 30°C in an incubator for 7 days.

2.3 Results and Discussion

There have been many studies with copper (II) chromate LPs on the literature [30] [35]. Previously our research group had produced these LPs on polyacrylamide (PAM) to investigate the effects of temperature of the external environment, and the mechanical deformation of the medium [30] [33]. Here we choose this LP system due to its ease of preparation and fast formation of the pattern (i.e. span of days).

PAM hydrogel was the ideal choice for temperature and mechanical deformation studies due to its high glass transition temperature and extended

elastic properties. However in this study we shifted our attention to biodegradable and non-toxic media.

Even at low concentrations agarose has good mechanical properties, allowing us to cut pieces without damaging it. Due to these reasons we choose to use agarose as the medium. Our inner electrolyte is K_2CrO_4, and the outer electrolyte is $CuSO_4$.

Although medium is an important factor for the formation of LPs, there are limited studies on it. Previously Ibrahim et al. mixed gelatin and agarose together and produced $Ag_2Cr_2O_7$ LPs [39]. They observed that by altering the either of the hydrogel concentrations they can alter the widths of the LPs. Sherif et al. determined that once they increased the gelatin concentration from 5% to 9% w/v, the number of produced rings decreased [40].

2.3.1 Agarose Concentration Changes the Spacing Coefficient of Copper Chromate Patterns

First, the effect of medium concentration on the homogenous samples were investigated. Therefore the LPs on agarose concentrations of 1.0, 2.0, 3.0, 4.0, and 5.0 % w/v were prepared.

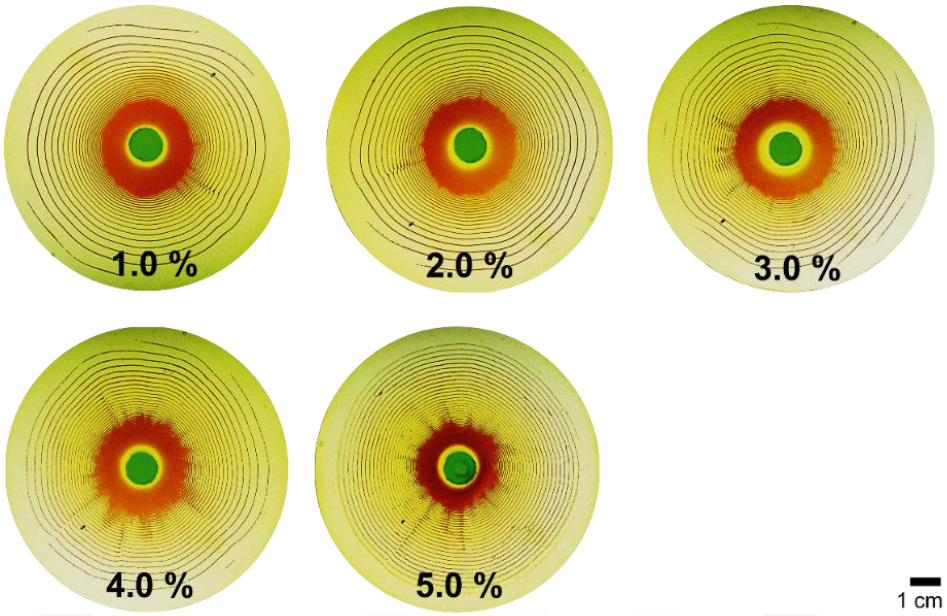

Figure 5. The effect of agarose concentration on the production of $CuCrO_4$ patterns. In all samples $[K_2CrO_4]$ = 0.10 M (inner electrolyte) and $[CuSO_4]$ = 1.0 M (outer electrolyte). Pattern formation was tracked for three days.

Once we increased the agarose concentration from 1.0 to 5.0 % w/v, the LPs began to form more closely to one another, and the spacing coefficient of the system decreased (Figure 6). The decrease of spacing coefficient can be attributed to the decrease of porosity with the increase of gel concentration [57].

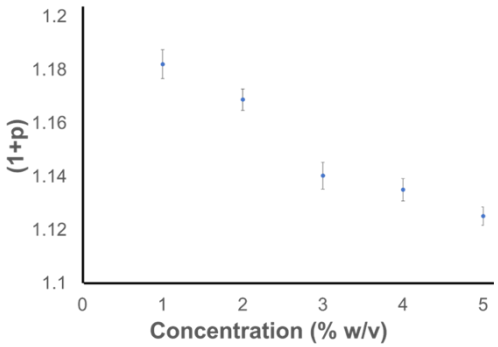

Figure 6. The effect of agarose concentration on the spacing coefficients of the $CuCrO_4$ LPs, an increase in the concentration of the agarose leads to a decrease in the spacing coefficient.

2.3.2 Agarose Concentrations Changes the Particle Size of the Product in Copper Chromate Patterns

Here our aim is to understand the effect of concentration on the particle size. To make such analysis we analysed the particle morphology of the first 6 rings. Beyond this ring number we cannot see the individual particles since clusters begin to form. To distinguish the regions of rings ,and non-ring, we applied elemental analysis with EDX. While there is a small peak corresponding to Cr in the ring region, such peak is not present in the non-ring region ,and we used it to separate two regions from one another.

To make a particle size analysis, we randomly choose 50 particles from the SEM micrograph ,and measure the areas of the particles with Image J software. The areas of particles can be approximated as circles then we calculated the diameters. Below we denote the effect of concentration on the particle morphology of the rings 1 and 6.

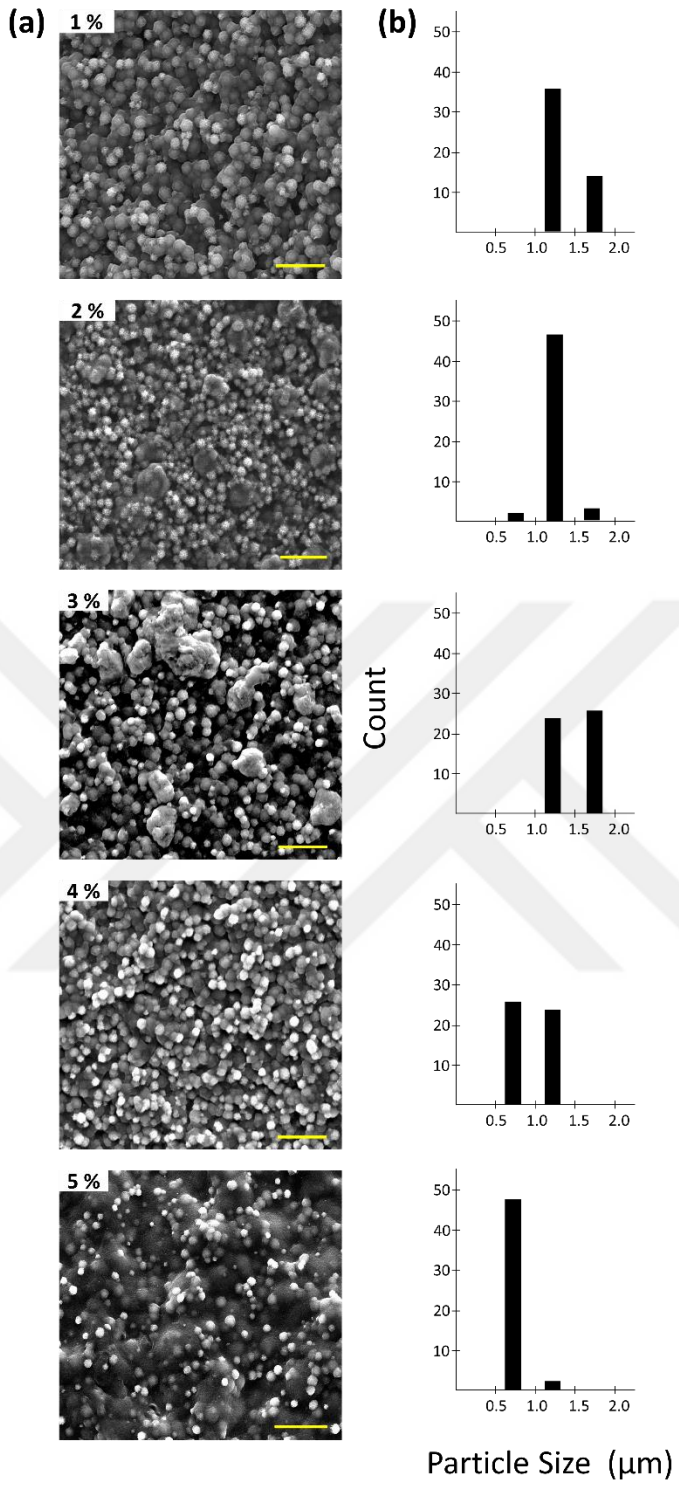

Figure 7. (a) SEM micrographs of **ring 1** on agarose hydrogel from samples of different concentrations from 1.0 to 5.0 % w/v. (b) The histograms denoting the particle size distribution. The scale bar is 5 µm. The error bars are calculated from the standard deviations of the distribution.

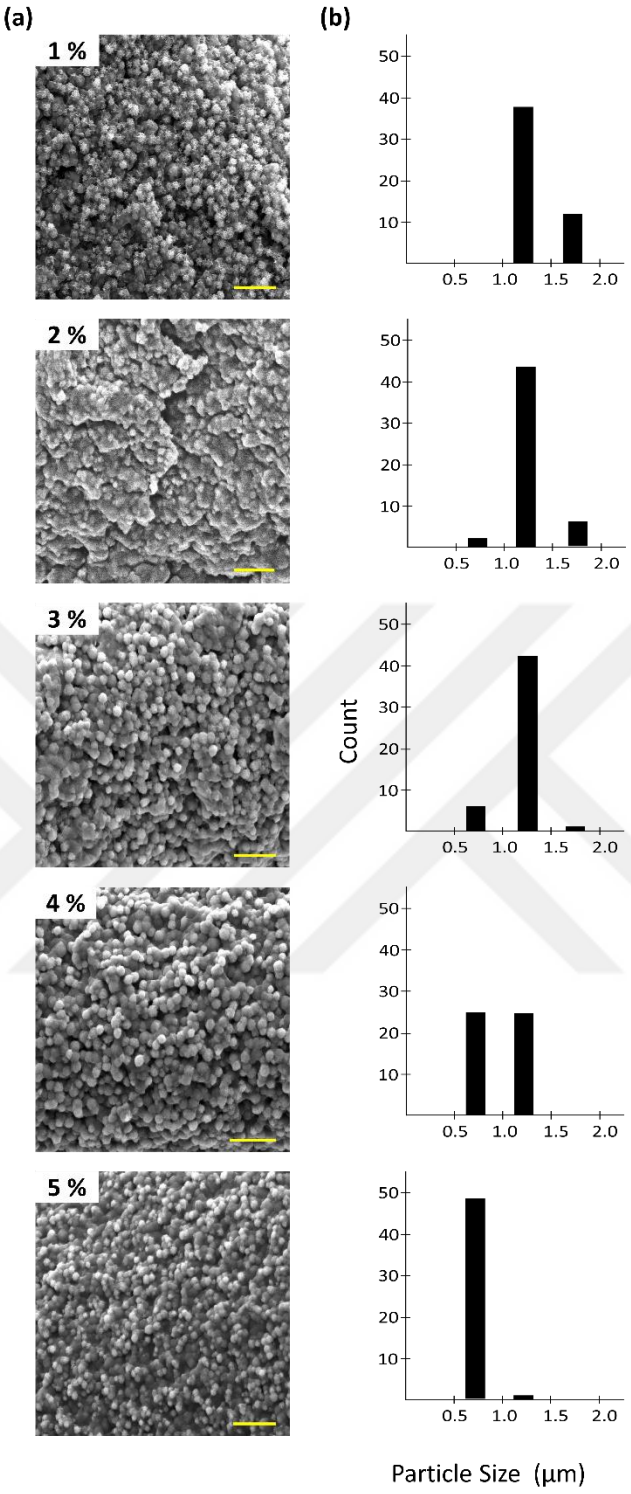

Figure 8. (a) SEM micrographs of **ring 6** on agarose hydrogel from samples of different concentrations from 1.0 to 5.0 % w/v. (b) The histograms denoting the particle size distribution. The scale bar is 5 µm. The error bars are calculated from the standard deviations of the distribution.

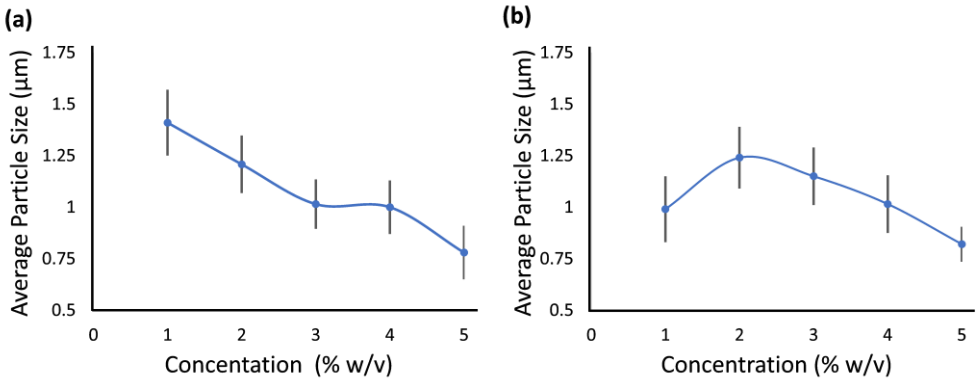

Figure 9. Average $CuCrO_4$ particle size of (a) ring 1 and (b) ring 6 at different concentrations of agarose within the range of 1.0 to 5.0 % w/v. Error bars are calculated from the standard deviations of the distributions.

We expected to observe a decrease in the average particle size with an increase in the gel concentration. However, the average particle size decreased for ring 1 and stayed the same for ring 6 (Figure 9).

2.3.3 Effect of Geometry of the Shape on the Spacing Coefficient

Here in this study, we have added an additional complexity to our artificial system. Previously our research group has worked with heterogenous systems, in which they only changed one parameter from the external environment [30] [33]. In a previous study, Fialkowski et al. showed a change in the LPs when the diffusion front travelled from thicker to thinner regions [41].

In this study we created both a heterogenous system by preparing regions of different agarose concentrations within the same petri dish, and additionally we added an element of geometry (Figure 10). We selected 4 different geometries for the shape of the boundary, triangle, square, pentagon, and circle.

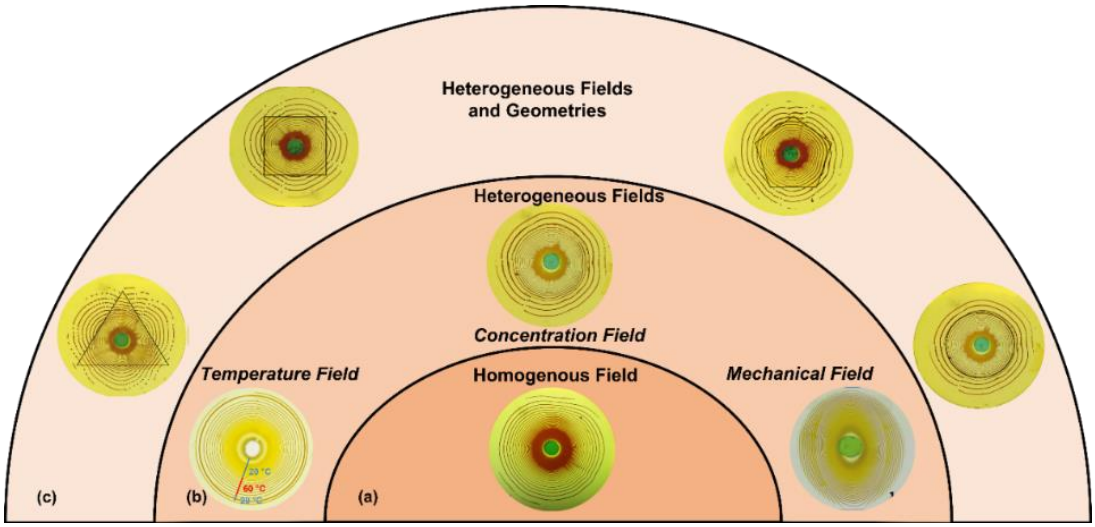

Figure 10. The increasing complexity of $CuCrO_4$ LPs forming in hydrogels. (*Centre to out*) (a) The LP formation in a homogeneous environment produces only regular LPs – concentric rings obeying spacing laws. (b) Patterns forming in heterogeneous fields lead to more complex LP patterns. Temperature change (low-high-low), or mechanical field change (stretch-release) were previously shown to yield deviations from the LP spacing rules. These deviations can be used to track back the environmental changes during LP formation. (c) A change in the concentration field with geometrical boundaries adds complexity to the patterns [42].

The next task was to determine the concentrations of inner and outer regions. We choose the concentration of the inner region 5.0 % w/v and the outer region 0.5 % w/v.

To compare the effect of the shape of boundary on the pattern formation, the shapes had to be of the same surface area. For this first we selected the areas of the shapes to be 16 cm^2. This area allowed us to observe more than 15 LPs within the inner region, which allowed the spacing coefficient calculations to be more accurate.

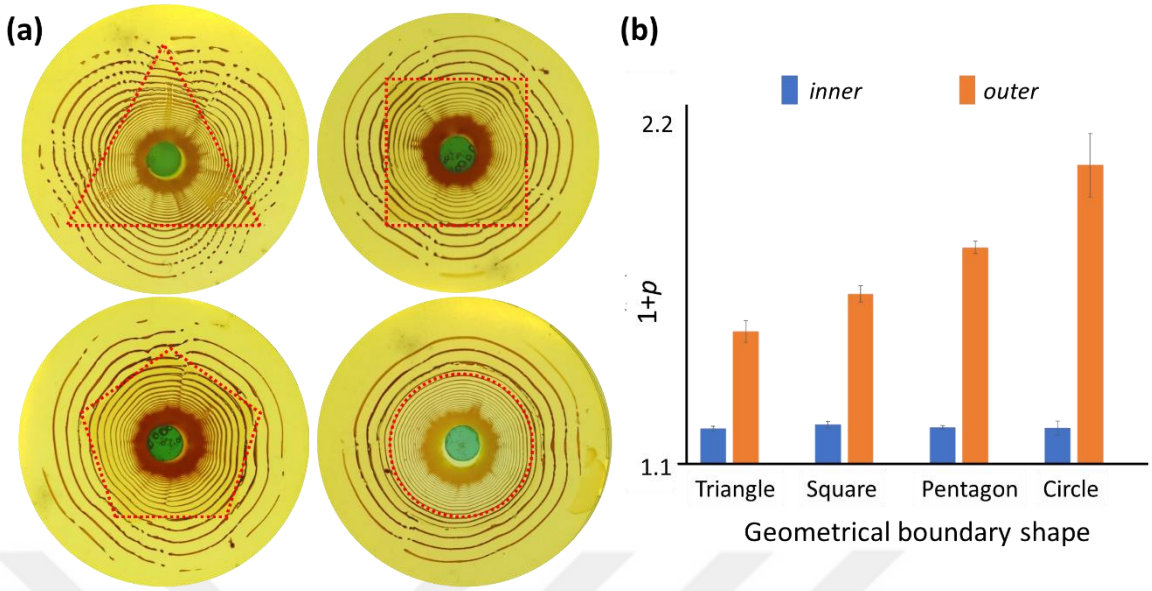

Figure 11. (a) The effect of polygon shape on the spacing coefficient in high ,and low concentration regions. (b) The spacing coefficients in the inner (5.0% w/v, blue) ,and outer (0.5% w/v, orange) regions of the polygons. LP patterns change their spacing coefficient entering the lower gel concentration region. The circular boundary region affects the greatest changes in the spacing coefficient. In all samples: [K_2CrO_4] = 0.10 M (inner electrolyte) and [$CuSO_4$] = 1.0 M (outer electrolyte), *t* = 3 days. Error bars denote the standard deviation from at least five independent measurements [42].

We calculated spacing coefficients of the inner and outer regions separately and then compared the corresponding values. As expected, spacing coefficient of the inner regions for all shapes were lower compared to outer regions ,and we could not observe a significant difference between different shapes, which we expected to see. For the outer regions, spacing coefficient increased with the increased number of polygon sides (Figure 11).

2.3.4 Effect of Geometry on the Curvature

Further we observed that once the diffusion front passed from high to low concentration regions, rings were distorted, and the curvature of the LPs increased (Figure 12).

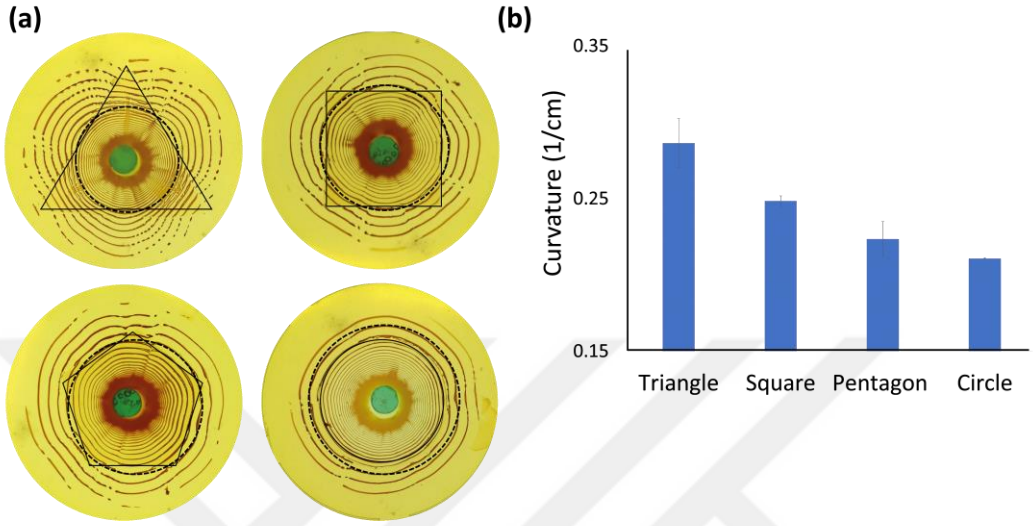

Figure 12. The effect of the physical boundary on the curvature of the produced LPs in the outer region (5.0% w/v) (a) The **dotted** lines denote the imaginary circles fitted to the first LP ring in the outer, less-concentrated region (b) The corresponding curvature values of the samples calculated by taking the reciprocal of the imaginary circle radii values in (a). [K_2CrO_4] = 0.10 M (inner electrolyte) and [$CuSO_4$] = 1.0 M (outer electrolyte), *t* = 3 days. Error bars denote the standard deviation from at least five independent measurements [42].

To calculate the curvature, we fitted an imaginary circle to the first ring in the outer region. Then we calculated the diameter of this circle and by taking the reciprocal of this value we determined the curvature. We determined that the curvature values for triangle, square, pentagon, and circle as 0.29 cm^{-1}, 0.25 cm^{-1}, 0.22 cm^{-1}, and 0.21 cm^{-1}, respectively.

2.3.5 Effect of Geometry on the Particle Morphology

Later we were curious on the effect of a physical boundary on the particle morphologies of the particles. To do that we focused on the last 2 rings of the 5.0% w/v region and the first 2 rings of the 0.5% region.

We observed that while the two rings forming before the rings developed beyond the boundary were spherical in shape, immediately when the boundary between the regions was passed particles were deformed. As demonstrated in Figure 8 below, while the particles on the rings 14 and 15 were mostly spherical in shape, at rings 16 and 17 we observed deformed spiky particles.

To understand the effect of the boundary on the crystal size, we compare the average particle size of the ring 1 of the homogeneous sample, and the ring 16 demonstrated in Figure 8. While for the homogenous sample, the average particle size 1.34 μm with a standard deviation of 0.24, for the ring 16 the average particle size is 0.68 μm with a standard deviation of 0.07. The change in morphology of the particles result in a significant decrease of the particle size. Based on our SEM analysis of the patterns forming in homogeneous-concentration samples (samples without any concentration borders), shown in Figure 9 above, we observe the spiky particles forming also in the homogeneous media of 0.50 and 1.0 % w/v agarose. The spiky particles were reported by Thomas et al. as well [43].

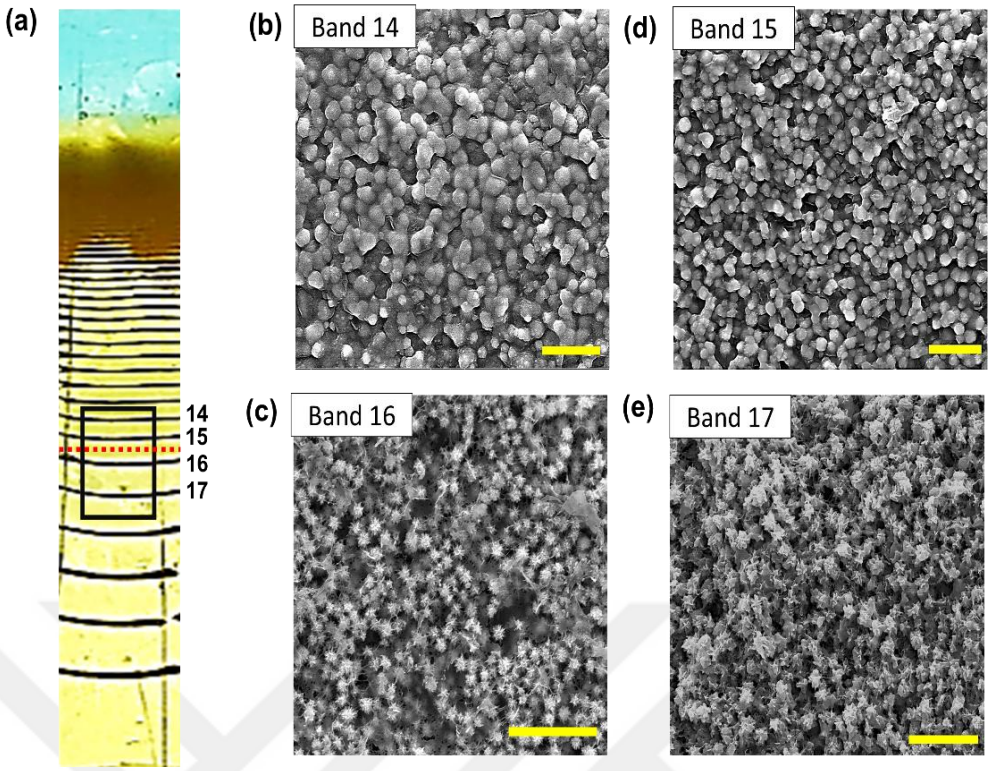

Figure 13. The LPs going through the concentration boundary can yield particles of different morphologies across the boundaries. (a) 1D $CuCrO_4$ LP system, (b-e) Scanning Electron Microscopy (SEM) micrographs of $CuCrO_4$ precipitates in LP bands in band 14 to band 17, respectively. The dashed red line denotes the boundary between the regions of different gel concentrations. The scale bar is 5 µm [42].

To understand why we have different particle morphologies at different concentrations, we employed X-ray diffractometry.

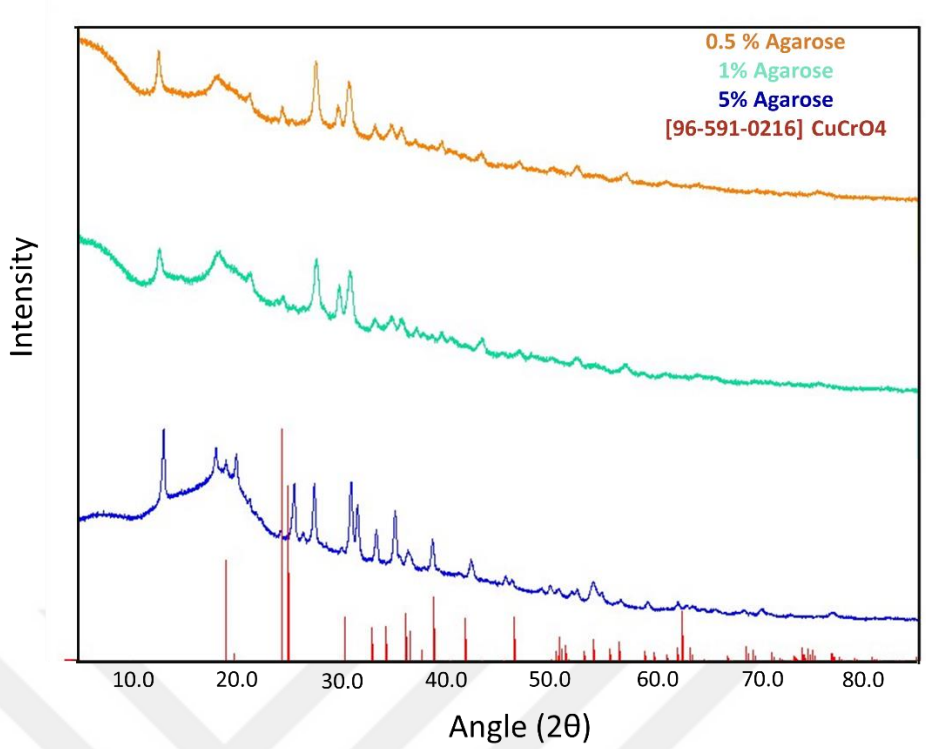

Figure 14. XRD diffractogram of copper (II) chromate particles developed on different concentrations of agarose 0.5 % w/v (orange), 1.0 % w/v (green) and 5.0 % w/v (navy) gel. The reference XRD diffractogram of $CuCrO_4$ is given in red [44].

However, we could not match the diffractogram pattern we obtained with the reference $CuCrO_4$ diffractogram pattern [96-591-0216] found on the Crystallography Open Database [44]. This difference can be attributed to the fact that the reported values in the literature belong to samples crystallized from a solvent. However, in our case, we have a crystal that develops in a gel medium. Since the interactions between the ions and the polymer chains can affect the formation of the crystal, the crystal structure might be different than those of the ones forming in solutions. Complete characterization of the structure of the crystals forming in the gel media and identification of the Miller indices of crystal planes are beyond the scope of this thesis. Therefore, they are not provided here.

2.3.6 The Model

The numerical model build by Gabor Hollo and Istvan Lagzi [42] depicted that the distances between the rings in the outer region are greater compared to the rings in the inner region. Further this model could predict the distortions occur once the diffusion front passes to high to low concentration. The least distortion occurs for the sample with the circular boundary like our experimental findings (Figure 11).

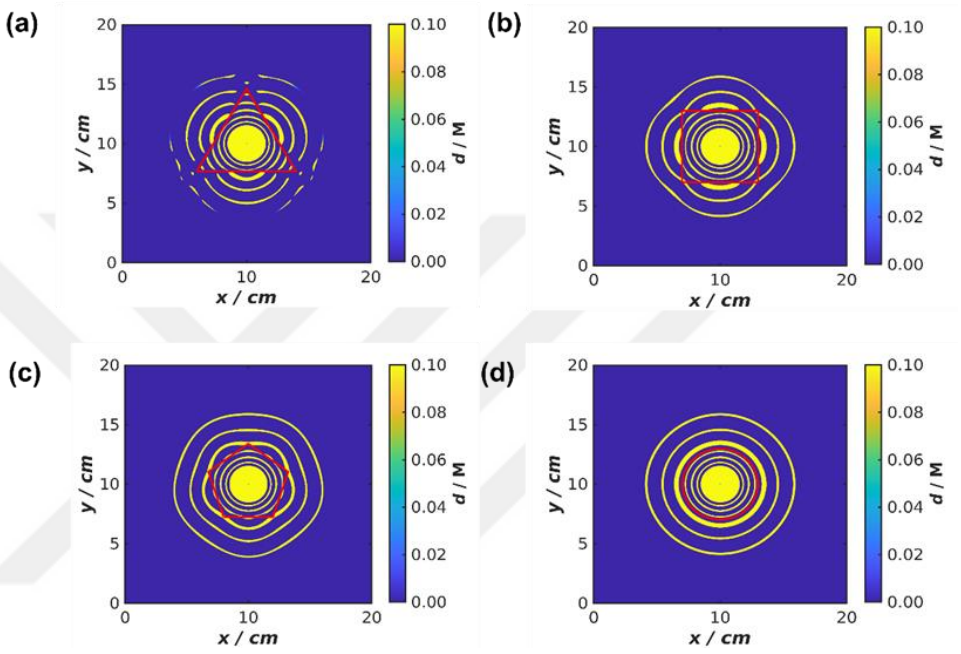

Figure 15. The numerical simulations of the LP development through the high gel concentration to the low gel concentration regions. The red line in (a-d) is the boundary shape [42].

Later by creating a planar front we investigated the similarities and difference of our system with physical waves. For this design we had two gel environments (0.50 and 5.0% w/v) and we combined the two of them together with a 45^{o} angle and investigated the pattern formation.

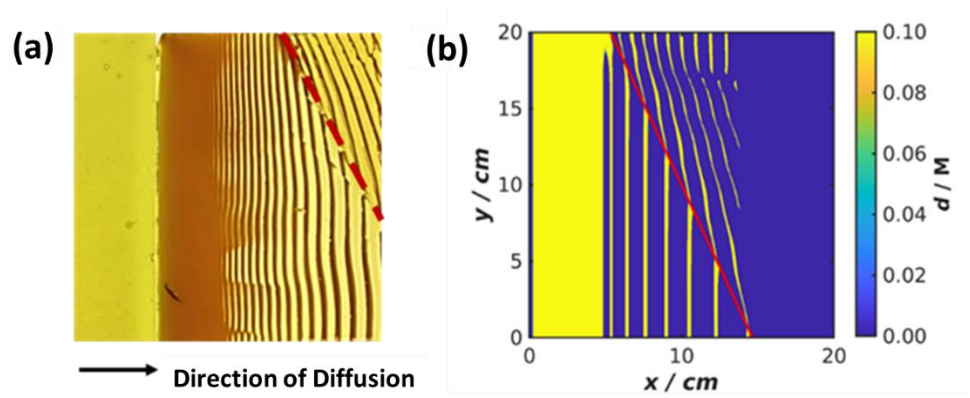

Figure 16. The refraction of the LP bands through a tilted boundary separating the high gel ,and low gel concentration regions in a 1D diffusion setup. (a) experimental result ,and (b) numerical simulation. The dotted red line denotes the boundary between the regions of 0.5 w/v and 5.0 w/v agarose. [K_2CrO_4] = 0.10 M (inner electrolyte) ,and [$CuSO_4$] = 1.0 M (outer electrolyte), pattern formation is tracked for 24 hours [42].

Originally the patterns are parallel, however they become tilted when the front moved to the boundary (Figure 16). This behaviour of the LPs is highly reminiscent of the physical waves, like when a wave passes from a region with high refractive index to low refractive index. Snell's law is used to understand the wave's path when it travels between regions. (Figure 17)

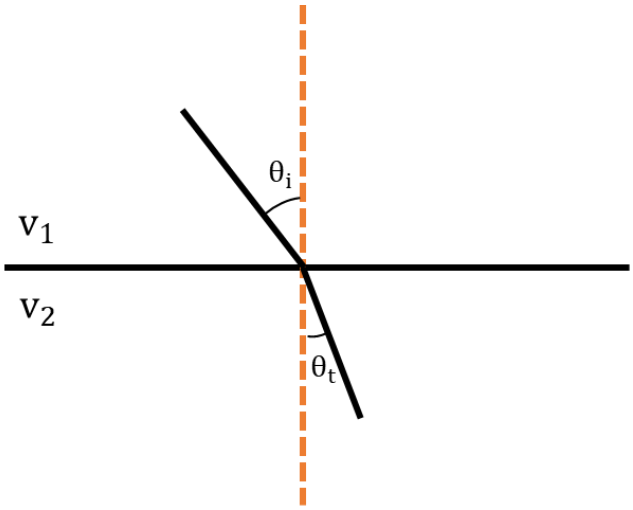

$$\frac{\sin\theta_i}{v_1} = \frac{\sin\theta_t}{v_2}$$

Figure 17. Schematic representation of the Snell's Law. v_1 ,and v_2 are the speeds of the waves in the respective media, θ_i is the incident angle, and θ_t is the transmitted angle.

Here in our system, we can draw a parallel between the high and low concentrations regions of the sample to high and low refractive indices of two neighbouring media, respectively. If a wave travels to a region of higher refractive index, the angle of incidence will be greater than the angle of refraction.

We observe the same with our experimental system. The angle of refraction was lower than the angle of incidence the diffusion front travels in the higher concentration gel environment. Hollo and Lagzi reproduced the same observation in a numerical simulation as well (Figure 16). Nevertheless, there is a significant difference between our artificial system and a physical wave. Once the physical wave enters to a region with different refractive index it is assumed that the speed remains constant. However, in a LP system which is a type of reaction – diffusion system the chemical front propagates with a decreasing velocity in the high concentration medium because the diffusion slows down in this medium.

2.3.7 The Effect of Gel Concentration Boundaries on a Biological System – Bacterial Growth Through the Boundary

As mentioned above, pattern formation is encountered in many different platforms in nature. After finding that a simple concentration barrier has a significant affect in pattern formation in an artificial system, the possible effects of such a barrier on a biological system was also investigated. For this purpose, we chose to work on simple and well-known biological systems of bacterial colonies.

In literature there are studies on how the bacteria growth pattern changes when bacteria are grown in different agar concentrations. The agar concentration governs the rate the bacteria can proliferate. In high agar concentrations bacteria can hardly proliferate, however in lower concentrations of agar they can proliferate easily [45].

Common bacteria growth morphologies are, diffusion-limited aggregation (DLA), dense-branching morphology (DMB), concentric rings, and Eden-like growth [45].

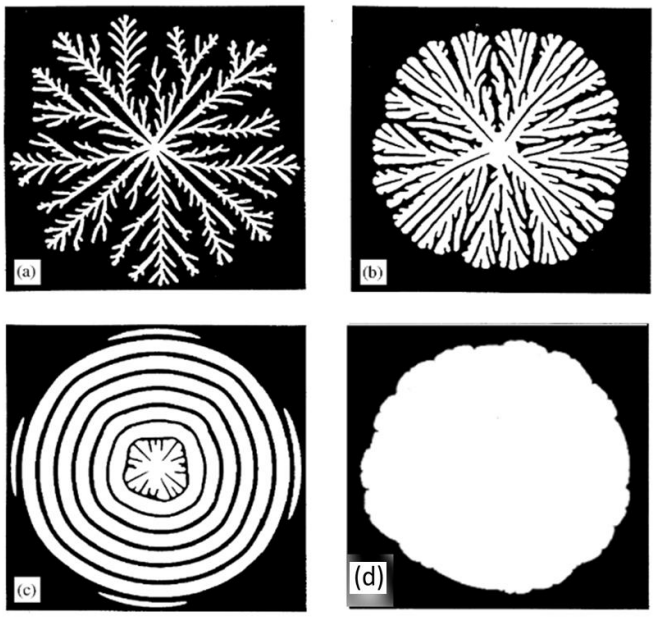

Figure 18. Common growth patterns of bacteria, (a) diffusion-limited aggregation (DLA), (b) dense-branching morphology (DBM), (c) concentric ring morphology (d) eden-like ring morphologies. The image is reproduced from [45].

We chose to work with *Bacillus subtilis* (strain DSM 1971), which is a model organism to study cell division, protein secretion, surface motility, and biofilm development [46]. The Lysogenia Broth (LB) medium is a nutrient rich medium is commonly applied to cultivate bacteria. There are four components of the LB medium, and these are NaCl, tryptone, yeast, and agar. Sodium ions, which are necessary for transport and the osmotic balance are provided by sodium chloride. Tryptone provides the essential amino acids such as peptides, and peptones. Yeast is necessary to provide a plethora of organic compounds which are helpful for bacteria growth, and agar is the medium that the bacteria can set [16]. We prepared the samples as detailed in Section 2.2.6 to probe these parameters ,and the effect of gel concentration boundaries on the bacterial growth.

All four parameters must be investigated to find a proper system of study to observe the growth of bacteria before preparing systems with concentration boundaries. Therefore, we studied the grow characteristics of the *Bacillus subtilis* by varying the concentrations of agar ,and tryptone. We analysed the bacteria growth in four different tryptone concentrations 0.5, 1.0, 1.5 ,and 2.0 % w/v. In all the given tryptone concentrations, we also prepared five different agar concentrations 1.0, 1.5, 2.0, 2.5, and 3.0 % w/v. Bacteria solution is planted in the middle of the boundary of the regions.

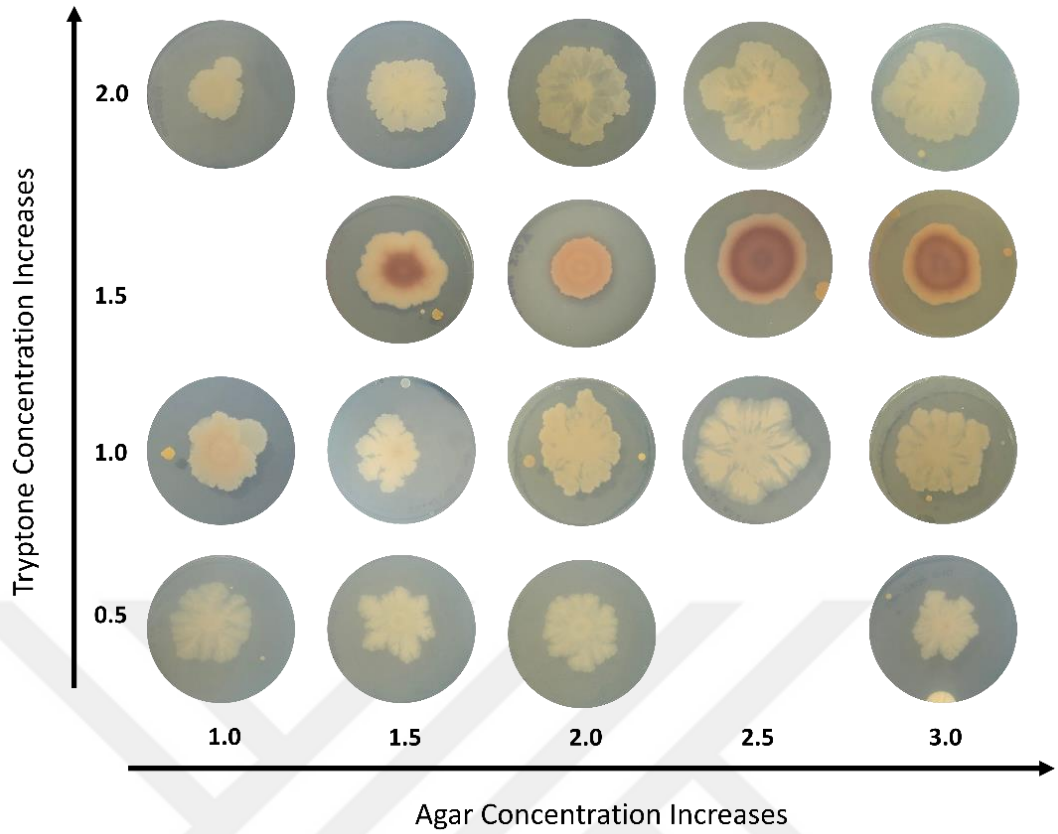

Figure 19. Effect of agar and tryptone concentrations on the morphology of bacteria growth. Pattern formation is tracked for 7 days.

As shown in Figure 19, when the tryptone concentration is 0.5 – 1.0% w/v, we observe DMB type morphology for all agar concentrations. When the tryptone concentration is 1.5% w/v, we observed concentric ring formation. When the tryptone concentration is 2.0 % w/v, we only observe Eden type growth at all the agar concentrations. As the concentration of tryptone increases, the pattern morphology shifts from DMB to Eden-like.

Fujikawa demonstrated that DLA type growth is observed at low concentrations of nutrients. The DLA colony grew in the direction of higher peptone levels (i.e., the nutrient) in an agar plate. Once the concentration of nutrient increases but at the same agar concentration, branches of the DLA colony becomes thicker ,and smoother, and the morphology becomes rounder, ,and we observe Eden type growth. They obtained DBM type growth once they increased both the concentrations of nutrients and agar [48]. From our studies, we could not form a

clear relation between the tryptone, and agar concentration on the bacteria growth morphologies.

From the above presented results (Figure 19), we selected the constant tryptone concentration of 1.0 w/v to prepare the samples with agar concentration boundaries. This value was chosen because it is the standard concentration of tryptone in LB medium. Further we kept the concentration of the inner region to be 1.0 % w/v, because it was the lowest agar concentration, in which bacteria grew fastest. When we tried the same experiment with 0.5 % w/v, instead of 1.0 % w/v, plates melted in 2 days after they were kept in an incubator. This is due to the low mechanical strength of the plates.

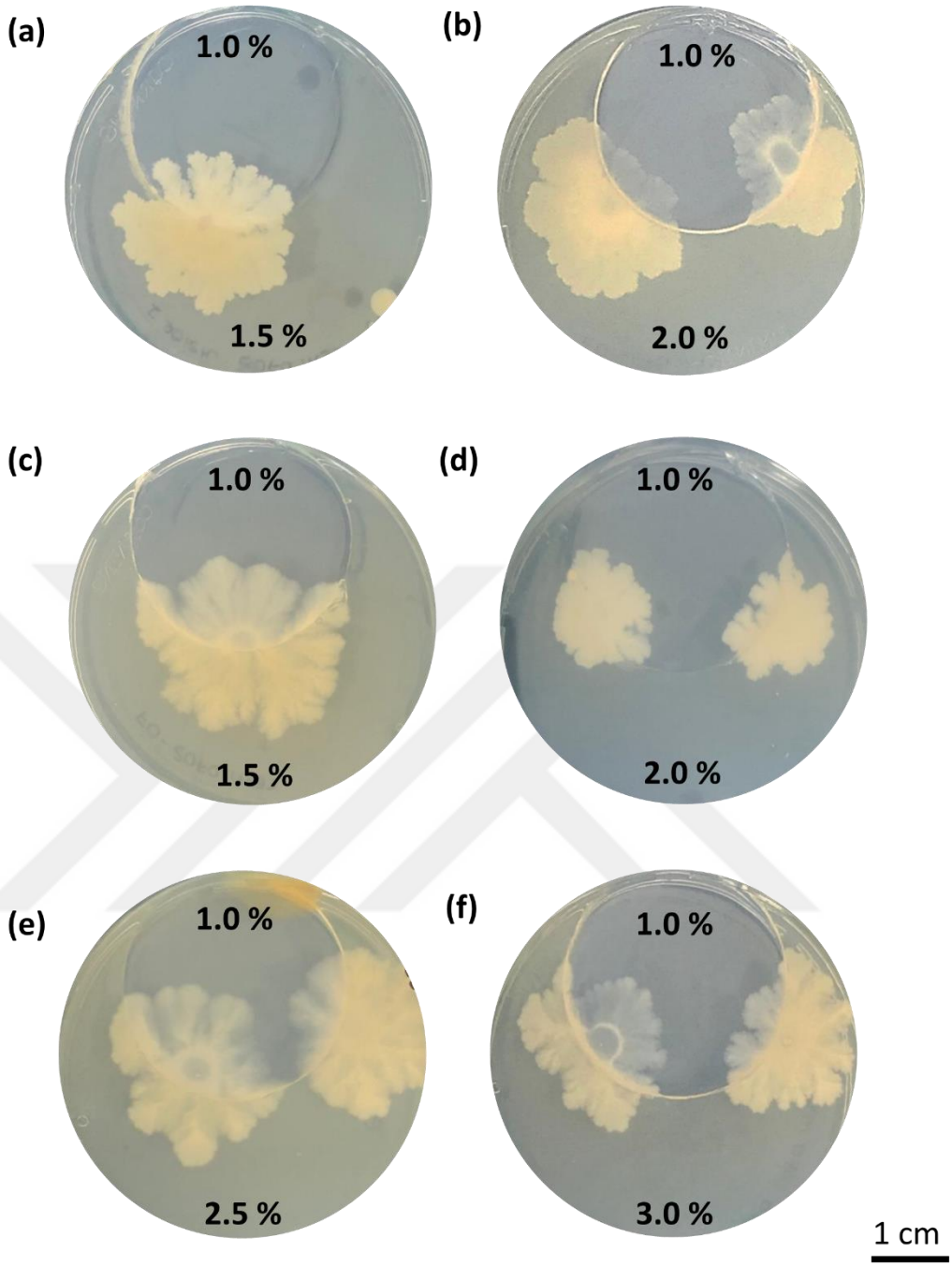

Figure 20. Bacteria growth evolution on different gel concentrations through a spherical boundary (a) 1.5 % w/v agar outside, (b) 2.0 % w/v agar outside, (b) (a-b) 1.0 % w/v agar inside , tryptone = 2.0 % w/v, (c) 1.5 % w/v agar outside (d) 2.0 % w/v agar outside (e) 2.5 % w/v agar outside (f) 3.0 % w/v agar outside (c-f) 1.0 % w/v agar inside , tryptone = 1.0 % w/v. The agar concentrations are denoted on the figure as well. Pattern formation is tracked for 7 days.

For A ,and B, as we crossed boundary, we observe DBM type growth on the inner circle ,and EDEN type growth on the outer circle. For (C- F), we don't observe a change in the morphology between the regions. These results are demonstrated on Figure 20.

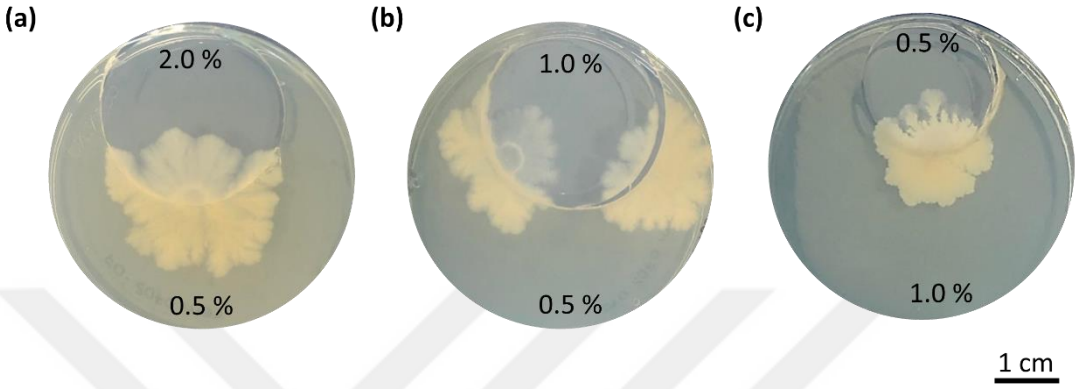

Figure 21. Bacteria growth evolution on different gel environments (a) 2.0 % w/v tryptone inside ,and 0.5 % w/v tryptone outside, agar is 2.0 % w/v for both regions (b) 1.0 % w/v tryptone inside ,and 0.5 % w/v tryptone outside, agar is 1.0 % w/v for both regions (c) 0.5 % w/v tryptone inside ,and 1.0 % w/v tryptone outside, agar concentration is 1.0 % w/v in both regions. The tryptone concentrations are denoted on the figure. Pattern formation is tracked for 7 days.

For a and b, we do not see any changes in terms of morphologies when the border is crossed. However for c we observe an EDEN type of growth, there is an almost DLA type of growth in the inner region. This is an interesting result because in single gel environment at the same concentrations we observed DBM type growth. This result could be an indication of adaptation capability of bacteria in the presence of a boundary.

Chapter III

3. Tracking of Temperature on Pattern Formation

In this chapter, we describe the preparation of magnesium hydroxide Liesegang patterns on agarose, PVA ,and gelatin ,and the characterization of the LPs. Finally, we display the effect of temperature ,and gel chemistry on the spacing coefficient, the morphology, and the average particle size of product in the patterns.

3.1 Materials

Agarose (Fisher Bioreagents for analysis purposes), gelatin (Carl Roth), polyvinyl alcohol (PVA) (Aromel Biomedical), magnesium sulphate (Fisher reagents) ammonium hydroxide (Sigma Aldrich 25-30%), magnesium chloride (Fisher reagents), sodium hydroxide (Emsure), glutaraldehyde (GTA) (Alfa Aeser)

Parafilm ,and Plexiglass were used without any chemical modification.

3.2 The Experimental Method

3.2.1 Preparation of 1D Gels

Preparation of $MgSO_4$ Doped Agarose Hydrogel

0.20 grams of agarose ,and 0.12 grams of magnesium sulphate were dissolved in 10 ml of distilled water, by heating the contents of the solution in a microwave. Then the pre-gel solution was poured into glass Pasteur pipettes ,and let to solidify at room conditions overnight. After complete gelation 1 ml of 15 M NH_4OH solution was introduced from the top of the gel.

Preparation of $MgSO_4$ Doped PVA Hydrogel

0.5 grams of PVA ,and 0.12 grams of magnesium sulphate were dissolved in 10 mL distilled water by heating ,and stirring the contents of the solution at 95 ^oC ,and 900 rpm. After complete solubilization, the pre-gel solution is acidified with addition of 3 drops of concentrated HNO_3 ,and 100 µL of GTA is added as crosslinker. Then the pre-gel solution is poured into one- dimensional pipettes ,and let to solidify at room conditions. Later 15 M NH_4OH solution is placed on the top of the pipette.

Preparation of $MgSO_4$ Doped Gelatin Hydrogel

0.5 grams of gelatin ,and 0.12 grams of magnesium sulphate were dissolved in 10 mL by heating ,and stirring the contents of the solution at 90 ^oC ,and 800 rpm. After complete solubilization the pre-gel solution is poured into one- dimensional pipettes ,and let to solidify at room conditions. For the chemically crosslinked gelation samples, 100 µL of GA crosslinker is added to the pre- gel solutions. Later 14.68 M NH_4OH solution is placed on the top of the pipette.

3.2.2 Determination of Magnesium Hydroxide Solubility Constant

20.33 grams of magnesium chloride ,and 4.04 grams of sodium hydroxide were dissolved in 200 ml of doubly distilled water separately. The solution of sodium hydroxide was slowly added to the magnesium chloride solution in a volumetric flask. The contents of the flask were stirred for 6 hours. Magnesium hydroxide was then filtered with vacuum filtration. Then the precipitate was washed eight times with 100 ml water. Magnesium hydroxide was then transferred to a mortar, crushed down to a fine powder, and dried overnight under vacuum.

0.020 grams of magnesium hydroxide was weighed in a glass vial ,and 5 ml of water was added. A total of five samples were prepared for each temperature value. Then the vials were transferred to a water bath at the desired temperature. The contents of the vial were stirred with a teflon coated magnetic stirring bar for six hours. Then the pOH of the solutions was measured with a pH meter, immediately after removing the vials from the oil bath.

3.2.3 Temperature Control Setup

The temperature was controlled with a DIY set- up using a Peltier element. A Peltier element can transport heat by using the Peltier effect. We used TEC1-12706 with the maximum current of 6.4 amps ,and a maximum voltage of 14.4 V, in our system. Both sides of the Peltier element were coated with a silicon-based thermal paste ,and placed in the middle of a heat sink ,and an aluminium plate. A thermocouple was placed between two plexi glass sheets. Here we used a κ- type thermocouple that works within the range of -20 to 80 ^oC. We converted the analog readings to the digital with an Arduino Nano using MAX-6675. Peltier 17 Driver used

in our setup was a half-bridge, BTS 7960B DC Motor driver. The BTS 7960B DC Motor driver had a maximum current rating of 40 Amps ,and the voltage working range was between 5.5 to 27.5 Volts.

3.2.4 Image Processing and Analysis, and the Determination of the Spacing Coefficient of the $Mg(OH)_2$ LPs

Identical to the Section 2.2.4; the data were extracted using ImageJ software. LP characterization was conducted using the Gray-value (pixel brightness, in the range of 0 to 225 in ImageJ software; gray-value = 0.229 × red + 0.587 × green + 0.114 × blue). Data collected using ImageJ was processed in MATLAB using a self-written MATLAB code exploiting the "Findpeaks" function to find the peaks' intensity, position, width, and *prominence* (the difference between the gray value of bands ,and their neighbour depletion zone). The spacing coefficient of the patterns signal ($x_{n+1}/x_n = 1 + p$) was retrieved from the slope of ln(x") vs. n, where x" ,and n are the position of the precipitation band ,and the band number, respectively, and $\ln(x")/n = \ln(1 + p)$.

3.2.5 Scanning Electron Microscopy (SEM) and Energy Dispersive X-Ray (EDX) Analyses of $Mg(OH)_2$ LPs

Identical to the Section 2.2.5; the LP-hydrogel samples were placed in glass flasks. Then the glass flasks were transferred to a liquid nitrogen bath for 10 minutes. The frozen hydrogels were cut in half with a steel blade ,and dried at vacuum for 24 hours.

The surface morphology of products was imaged with Quanta 200F model SEM with an accelerating voltage of 10 kV ,and spot size of 5. Samples were coated with Au-Pd for imaging. The particle sizes were determined using the digital image analysis ImageJ software.

3.3 Results and Discussion

3.3.1 The optimization of the inner electrolyte source and its concentration for obtaining $Mg(OH)_2$ LPs with higher number of rings

In our LP forming systems, OH^- ions was let to diffuse into the Mg^{2+} containing gel prepared as described in the previous section in the Pasteur pipettes from the top. The diffusing OH^- ions reacted with Mg^{2+} ions homogeneously distributed in the hydrogel ,and a precipitate formed wherever the concentration product was higher than the threshold, stated by the solubility constant according to the following reaction equation,

$$Mg(SO_4)(aq) + 2NH_4OH(aq) \rightarrow Mg(OH)_2(s) + (NH_4)_2SO_4(aq)$$

For the source of Mg^{2+} as the inner electrolyte, the three candidates $MgSO_4$, $MgCl_2$, and $Mg(NO_3)_2$ produced the $Mg(OH)_2$ rings without significant difference. Therefore, $MgSO_4$ was used as the inner electrolyte in the further experiments. NH_4OH, was chosen as the outer electrolyte because it did not interfere with the gelatin like NaOH.

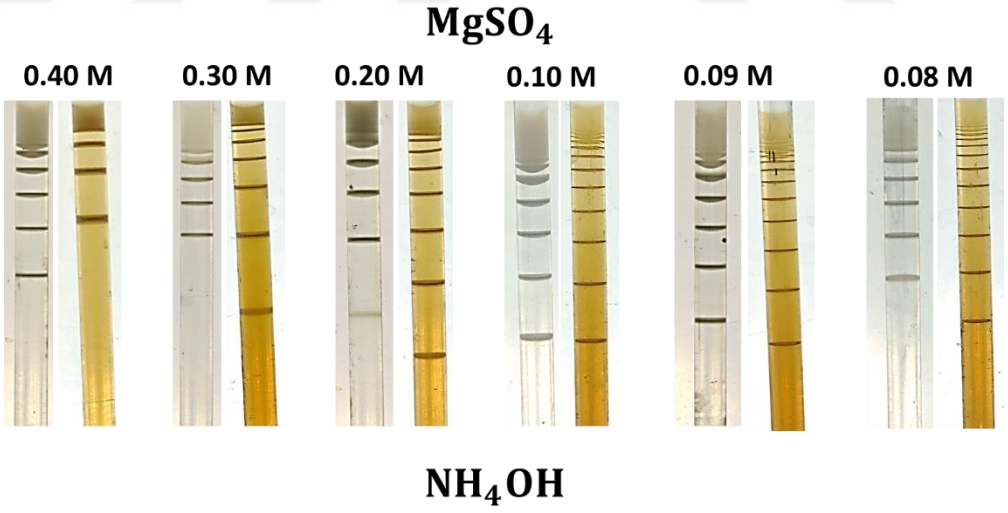

Figure 22. The effect of $MgSO_4$ concentration on the formation of $Mg(OH)_2$ LPs in gels without (left) and with (right) crosslinked 5.0% w/v gelatin. The inner electrolyte concentration was altered from 0.40 M to 0.08 M. $[NH_4OH]$= 15 M. The pattern formation is tracked for 24 hours.

We tried to optimize the concentration of $MgSO_4$ to obtain the highest number of bands forming at room temperature. A higher number of rings helps with accurate calculation of the spacing coefficient. In the optimization samples, we kept the concentrations of gelatin ,and the outer electrolyte constant at 5.0 % w/v ,and 15 M, respectively. Mg^{2+} concentrations, on the hand, were varied between 0.40 and 0.080. We used gelatin as the first gel medium in our study as most of the examples in the literature. Gelatin works very well for the formation ,and the display of LPs at room temperature and was adopted by many as reported in the literature. However, it is not mechanically strong ,and quickly disintegrates at temperature higher than 40 $^{\circ}$C. Glutaraldehyde (GTA) is a typical crosslinker to form a chemically crosslinked gelatin network. GTA is a five-carbon chain doubly terminated with formyl groups ,and with the presence of carbonyl groups, it is reactive towards primary amine groups ,and forms imine linkages [45].

To probe the differences of LP formation in gels with ,and without crosslinks, we prepared two sets of samples; in gelatin, ,and in GTA-crosslinked gelatin. $Mg(OH)_2$ LPs forming in the former showed no correlation between the number of bands forming or the band width of the rings, and Mg^{2+} concentration. In the crosslinked samples, decreasing the Mg^{2+} concentration increased the number of the bands ,and decreased the band widths in general, with a plateau around 0.10 M. Based on these observations, we decided to use 0.10 M concentration of $MgSO_4$. To be consistent, we used the same concentration of 0.10 M for $MgSO_4$ also in our preparations with PVA ,and agarose.

3.3.2 Testing Gel Medium Chemistry for Differences in $Mg(OH)_2$ LP Formation

We used PVA and agarose in addition to GTA-crosslinked gelatin to test the effect of the gel medium on the formation of $Mg(OH)_2$ LPs. Observing the positive effect of chemical crosslinking of the gel medium, we attempted to crosslink the PVA hydrogels as well. Although PVA hydrogels can be crosslinked physically with multiple freeze- thraw cycles [47], in our case this method did not work, and we could not observe gelation after 5 cycles. Since we could not physically crosslink the

PVA hydrogels, we attempted to chemically crosslink with GTA. The results of the LP formation in the three media are given in Figure 23.

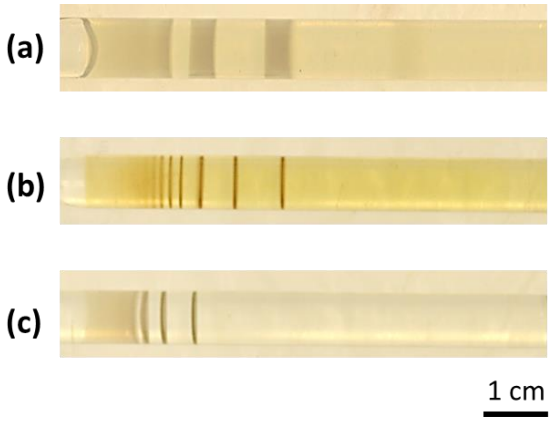

Figure 23. Formation of $Mg(OH)_2$ LPs on (a) agarose (b) GTA-crosslinked gelatin ,and (c) GTA-crosslinked PVA, in 24 hours. Pattern formation is tracked at 20 ^oC.

The number of rings developed within the same period of 24 hrs is higher in the crosslinked gels than those in agarose (Figure 23). However the spacing coefficients are lower in the crosslinked gels. Further we observe a significant difference in widths of the LPs. The widths of the LPs produced on agarose are much thicker compared to the ones on PVA and gelatin.

Porosity and the average pore size is an important factor to consider. Average pore size of agarose is larger than chemically crosslinked PVA and gelatin hydrogels [57] [59]. Typically a larger pore size leads to an increase in the diffusion of the outer electrolyte.

3.3.3 The Effect of Temperature on the Formation of $Mg(OH)_2$ LPs

Perhaps temperature is the most evident way to interfere with the Liesegang pattern formation. A change in temperature affects the diffusion rate, the precipitation threshold, and the reaction rate. These quantities are interconnected with each other too.

The relation between temperature and the rate constant is displayed in the Arrhenius equation. The relation between temperature and the diffusion coefficient is given in the Fick's Law of Diffusion. Both rate constant and diffusion coefficient

are directly related with temperature. However the solubility product may increase or decrease with increasing temperature. At room temperature (25 ^{o}C), the solubility product of $Mg(OH)_2$ is 5.6 x 10^{-12} [51].

We experimentally determine the effect of temperature on the solubility of our salt within the range of 25- 45 ^{o}C. For this purpose, we first formed our salt at room temperature and then redissolved constant amount of the salt in the pure water at the given temperature range above [52].

The dissolution of $Mg(OH)_2$ is assumed to occur as,

$$Mg(OH)_2 \rightleftharpoons Mg^{2+}(aq) + 2OH^{-}(aq)$$

We calculated the solubility product by measuring the pH of the solutions in which $Mg(OH)_2$ is redissolved. Then the calculated $[OH^-]$ values are used to compute the solubility constant K_{sp} at the corresponding temperatures shown in Table 1.

Temperature (^{o}C)	$\mathbf{[OH^-]}$ **(M)**	$\boldsymbol{K_{sp}}$
25	$1.66 \text{ x } 10^{-4}$	$2.29 \text{ x } 10^{-12}$
30	$1.38 \text{ x } 10^{-4}$	$1.31 \text{ x } 10^{-12}$
35	$1.05 \text{ x } 10^{-4}$	$5.28 \text{ x } 10^{-13}$
40	$0.892 \text{ x } 10^{-4}$	$3.55 \text{ x } 10^{-13}$
45	$0.676 \text{ x } 10^{-4}$	$1.54 \text{ x } 10^{-13}$

Table 1. The equilibrium $[OH^-]$ obtained by measuring pH of the $Mg(OH)_2$ redissolved at given temperatures.

The inverse relation between temperature and solubility can be explained by the fact that the dissolution of $Mg(OH)_2$ is exothermic. Here more energy is released to surroundings, than it is used in breaking up the solvent and solute molecules. As we introduce more heat to the system, dissolution of the salt decreases.

Once we determined the inverse relation between the temperature ,and solubility constant, we can predict that at higher temperatures the threshold for

precipitation will be lower ,and the precipitates will form sooner as the reactant diffuses into the gel leading to a decrease in the spacing coefficient [30].

To test this idea, we produced $Mg(OH)_2$ Liesegang patterns at 10-40 ^oC, in the three different hydrogels, agarose, crosslinked gelatin, and crosslinked PVA. As discussed in the previous section, we used the same inner ,and outer electrolytes concentrations and tracked the pattern formation for 24 hours for all types of hydrogels. The photos of LPs formed under these conditions ,and the corresponding spacing coefficients are displayed in Figure 24.

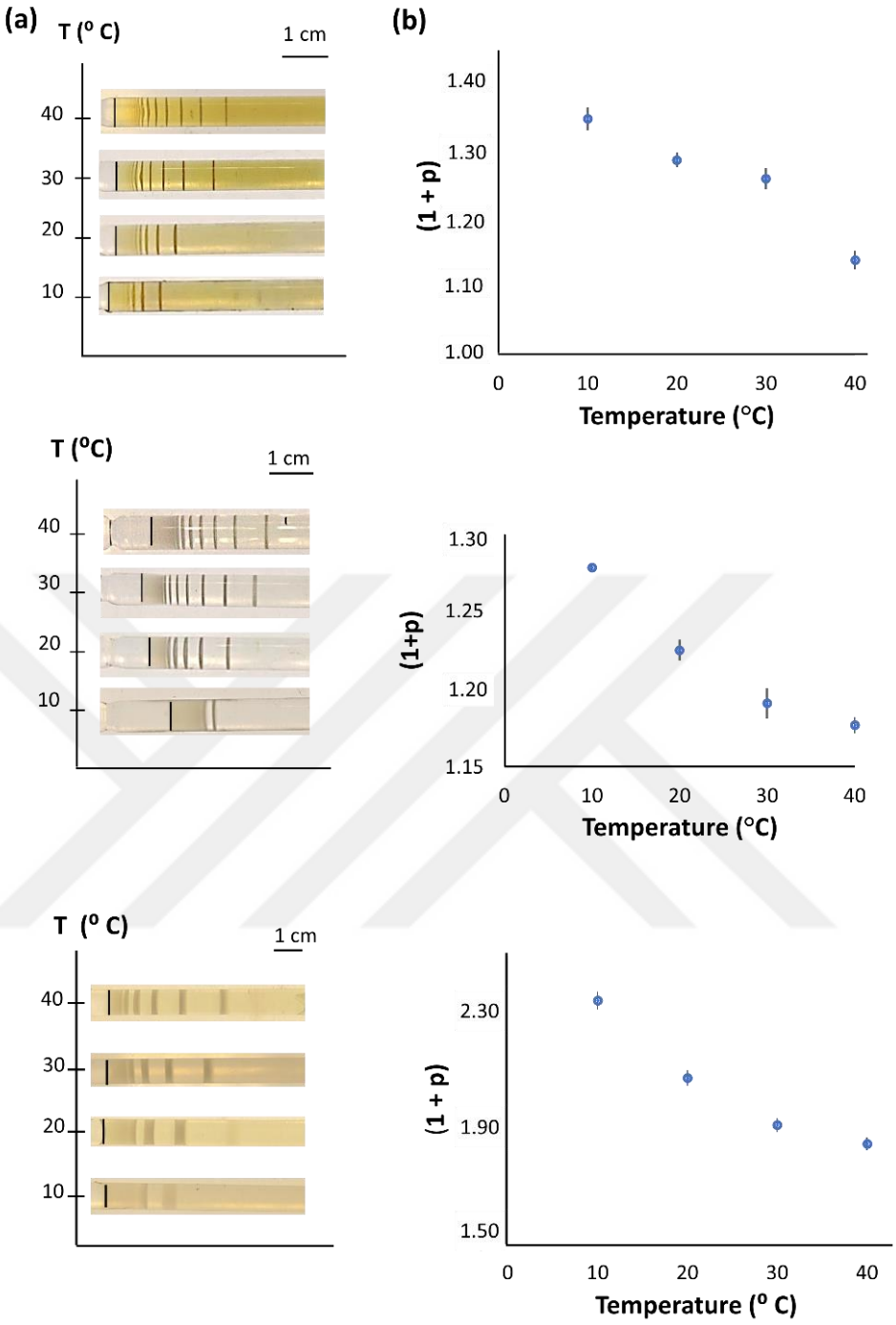

Figure 24. (a) Liesegang patterns formed at 10, 20, 30, 40 ^{o} C. Top to bottom: LPs developed in GTA-crosslinked gelatin, GTA-crosslinked PVA ,and agarose. The black line indicates the point of contact between the gel surface containing 0.10 M $MgSO_4$,and 15 M NH_4OH solution. (b) The variation of spacing coefficient in each of the samples at different temperatures. The error bars are calculated from the standard deviations of 5 samples. The pattern formation is tracked for 24 hours.

As expected, an increase in temperature led to higher number of rings produced in all gel media. Further our results supported our idea on the effect of the solubility on pattern production.

3.3.4 The Effect of Temperature on the Product Morphology and Particle Size of $Mg(OH)_2$ in the LPs

Depending on the synthesis method of $Mg(OH)_2$, diverse microstructures such as needles, platelets, rods, spheres, flowers, and stars of the salt can be obtained. The parameters affecting the microstructure are the nature of the base, temperature, chemical nature of the counter ion in the magnesium source, and whether the product is obtained through a hydrothermal treatment.

Sierra- Fernandez et al. reported formation of hexagonal $Mg(OH)_2$ particles from the hydrothermal reaction between $Mg(NO_3)_2$ and $N_2H_4.H_2O$ in a hydrothermal reaction. At 150 ^oC, they obtained hexagonal flakes with round corners however once they increased the reaction temperature to 180 ^oC, particle morphology changed to more regular hexagonal flakes [53].

Henrist et al. determined that when they used NaOH, the pH of the reaction medium exceeds the isoelectronic point of magnesium hydroxide particles in water. This results in, an exceeding overall negative charge on the surface of particles and a high supersaturation due to large concentration of hydroxyl ions [54]. Here we observe a fast nucleation process, and this leads to small ,and well- defined nuclei. These tiny ,and isotropic particles tend to aggregate in to lower their surface energy, ,and thereby they adopt globular type structure. In our LP system we observe such round morphologies especially in gelatin hydrogels.

In the same study, Henrist et al. observed formation of platelet-like $Mg(OH)_2$ particles when they used $MgCl_2$ as the magnesium source ,and NH_4OH as the base ,and at 60 ^oC. We observed such morphology with agarose at all temperatures. When they used NH_4OH, the pH of the solution is lower than the isoelectronic point (at around 10). Here particles are positively charged, thereby adsorption of crystals is not favoured. Due to larger size of ammonium ions, they cannot be adsorbed on

the facets of the crystals. Again, hydroxyl concentration is slightly excess in this case, and we again observe a fast nucleation [54].

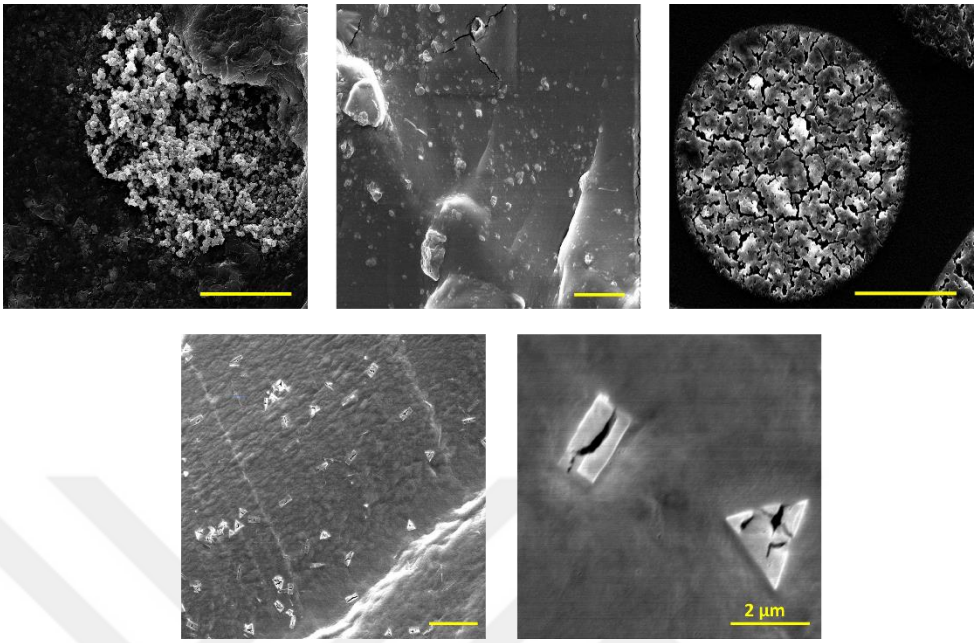

Figure 25. SEM micrographs of $Mg(OH)_2$ particles of different morphologies on GTA-crosslinked gelatin hydrogel. The scale bar is 10 µm except stated otherwise.

From analysing the band 1 and band 2 on the samples we found the following:

On gelatin, LP rings formed at various temperature were found to contain different morphologies of $Mg(OH)_2$, as displayed in Figure 29. Globular, irregular, cluster-like morphologies were accompanied by presence of rectangular , and triangular prisms. To the best of our knowledge, there are no reports on these latter morphologies in the literature. Due to these different morphologies coexisting , and the observed aggregation of the particles in crosslinked gelatin, we could not perform a particle size calculation for these particles formed in crosslinked gelatin.

We did not observe the diverse $Mg(OH)_2$ morphologies (Figure 25) on PVA and agarose hydrogels. The $Mg(OH)_2$ particles formed in the agarose hydrogel, had platelet shape (Figure 26), and they are reported in the literature as “sand rose” [54]. Tai et al. argued that SO_4^{2-} could be responsible for the formation of such morphology [55]. However, in our case we used the same inner electrolyte for all

our hydrogels and we observed this morphology only in products formed in agarose. The precipitates forming in PVA hydrogels had irregular shaped particles (Figure 29).

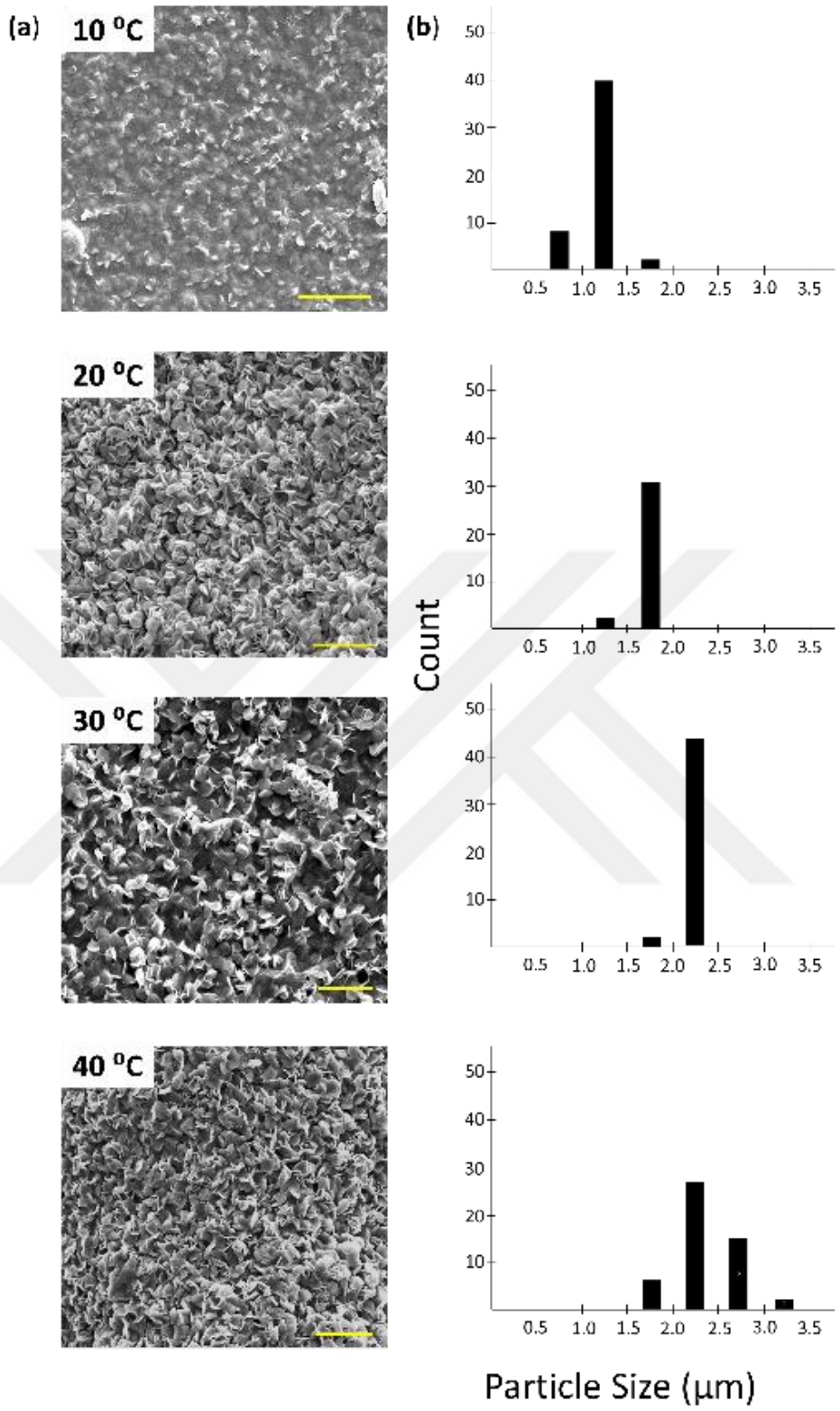

Figure 26. (a) SEM micrographs of band 1 on agarose hydrogel from samples at different temperatures 10-40 °C. (b) The histograms denoting the particle size distribution. The scale bar is 10 µm.

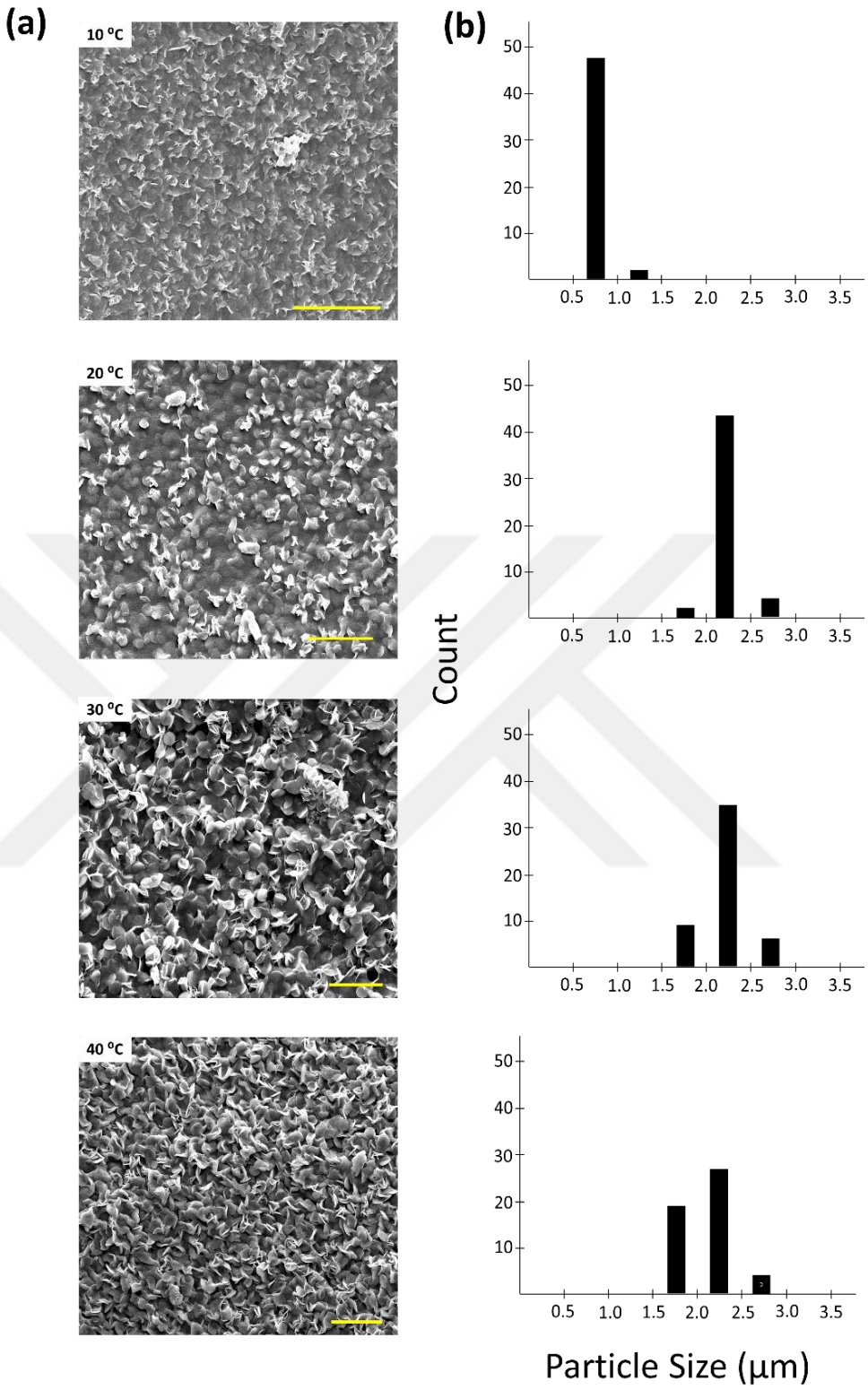

Figure 27. (a) SEM micrographs of band 2 on agarose hydrogel from samples at different temperatures 10-40 ^{o}C. (b) The histograms denoting the particle size distribution. The scale bar is 10 µm.

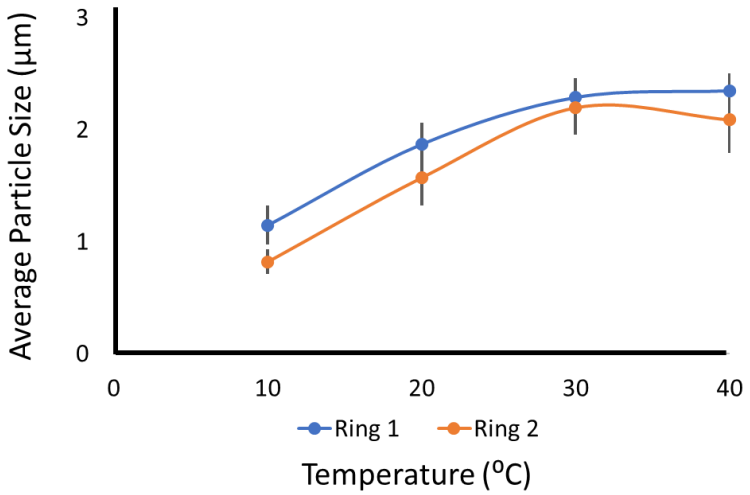

Figure 28. Average particle size in ring 1 (blue) , and in ring 2 (orange) on agarose hydrogel at 10-40 ° C. The error bars are calculated from the standard deviations of the distributions.

Supersaturation is the driving force for both the crystal growth and nucleation. At lower supersaturation typically crystal growth is observed and bigger particles form. At higher supersaturation crystal nucleation dominates over crystal growth, and formation of smaller particles is observed [58]. Based on this idea, we expected to see smaller particles when the solubility product is lower. Since the supersaturation will be high, the dissolution of colloids to form bigger aggregates will occur less likely [30]. Figure 28 displays that when the temperature increases, the average particle size increases – opposite to this hypothesis. This increase can be attributed to the weakened mechanical properties of the gel at higher temperatures, especially at 40°C

In other chemical systems [30], it was also shown that the particle size increases as the band number increases for the structures forming at the same temperature. In our system, at the same temperature (10-40°C) the average particle sizes are almost the same in ring 1 and ring 2. The further generations (ring 3 and on) had more clusters than individual particles, therefore it was hard to determine such a trend for this system.

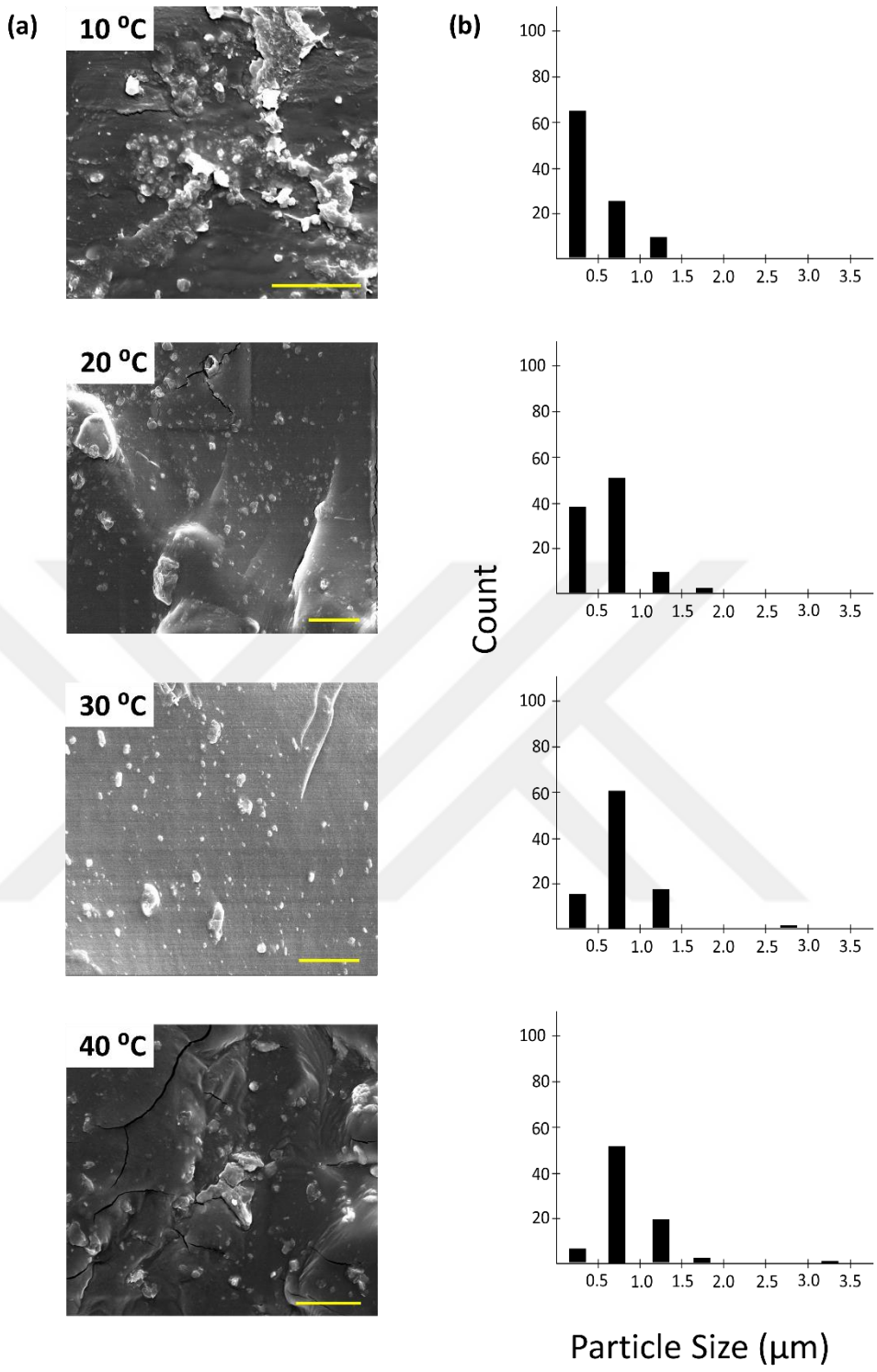

Figure 29. (a) SEM micrographs of **band 1** on GTA-crosslinked PVA from samples at different temperatures 10-40 °C. (b) The histograms denoting the particle size distribution. The scale bar is 10 µm.

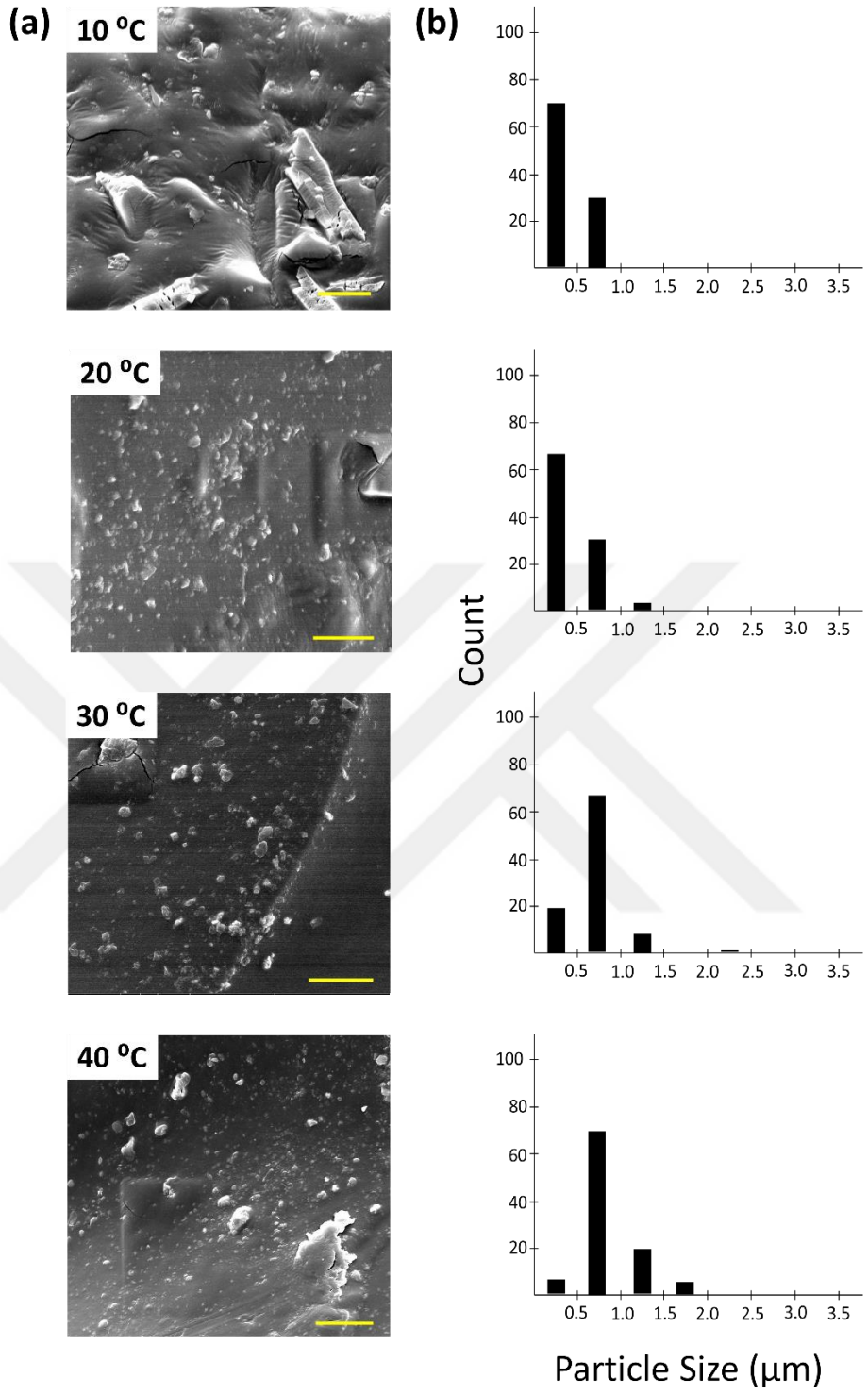

Figure 30. (a) SEM micrographs of **band 2** on GTA-crosslinked PVA hydrogel from samples at different temperatures 10-40 °C. (b) The histograms denoting the particle size distribution. The scale bar is 10 µm.

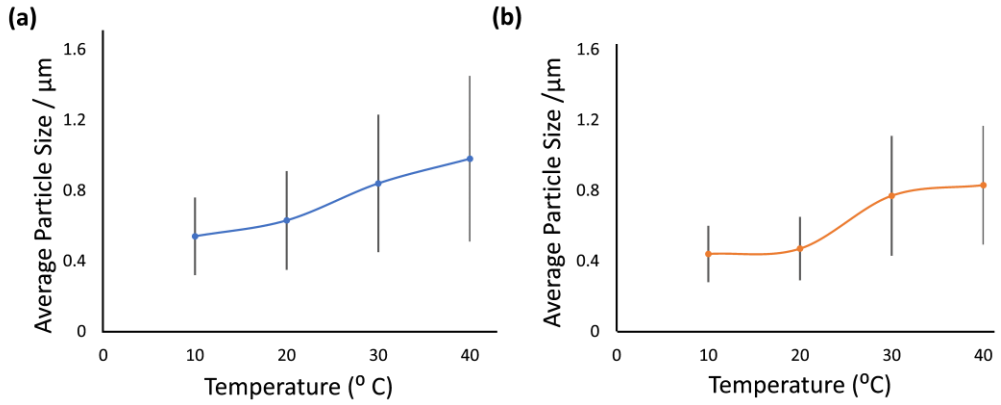

Figure 31. Average particle size in (a) in ring 1 and (b) in ring 2 on PVA hydrogel at different temperatures**.** The error bars are calculated from the standard deviations of the distributions.

For the PVA samples (Figure 29 and 30) we did not observe a pleated morphology. The particles were mostly in spherical shapes, with some big cluster formations especially at 10 °C. The reported particle size calculations (Figure 31) were not very accurate, since we mostly observed clusters instead of the individual particles. The cluster formation is the reason why we observe a significant standard deviation on Figure 31.

Conclusion

The main purpose of this thesis was to mimic complex natural , and synthetic pattern formation process with reaction diffusion systems, by breaking the symmetry of the systems. To achieve this aim in the first section of this work, regions of different concentrations are created, and the formation of $CuCrO_4$ LPs have been observed. In the second chapter, both the effects of temperature, and the medium are investigated through the $Mg(OH)_2$ LPs.

In the first section of this work, we demonstrated that chemical patterns could develop , and cause refraction of the pattern waves , and alterations in the band spacings through setting a boundary of different gel concentrations. The extent of the wave refractions depended on the geometric shape of the boundary. Although this refraction is like to the refraction of physical waves it cannot be explained entirely with the Snell's law. In the micro-level we observed a drastic change in particle morphology (spherical to spiky) when the RD system passed the boundary. These findings can also be used to program matter at both macro , and micro dimensions , and yield valuable insight to understand natural pattern formation processes. Our results from the short trial with a 'bio system' shows that the bio system with may (bio)chemical reactions take place at the same time is much different than the basic chemical reaction-diffusion systems with usually a single chemical reaction. However, the 'bio systems' respond to the definite 'barrier's in a visually trackable way – their responses are worth to study in detail to understand how the organisms (bacteria) proliferate in natural media.

In the second section of this work, we focused on producing $Mg(OH)_2$ LPs on different hydrogels (agarose, gelatin, and PVA) and showed the effect of the medium on the pattern production. We demonstrated that an increase in the temperature yielded a decrease in the spacing coefficient. The reaction rate between the magnesium and the hydroxide ions, and the diffusion coefficients of magnesium and hydroxide ions increase with temperature. However, the solubility product of magnesium hydroxide decreases with temperature. As a result, we obtained LPs form more closely to one another, at higher temperatures. The visual

appearance of the bands can be used to track down the temperature changes , and can be used as an environmentally friendly temperature tracking system.

The gel medium affected the $Mg(OH)_2$ particle morphologies. Especially on gelatin hydrogels diverse aggregations and particle shapes were observed. The morphologies produced on gelatin are not comparable with the morphologies observed on agarose and PVA. Additionally, the particle size increased in same-generation ring in higher temperatures and decrease in the next ring at the same temperature. Thus, by altering the hydrogel medium and altering the temperature a great variety of particles in terms of shape and size can be obtained. Understanding how these diverse morphologies form and the effect of the hydrogel environment on the particle growth may help to understand many heterogeneous reaction-diffusion systems, the precipitation and sedimentation processes in presence of (bio)polymeric media.

References

(1) Lenz, J.; Whitehad, A. N.; Price, L. Dialogues of Alfred North Whitead. *PPR*, **1955**, *15*, 441.

(2) Grzybowski, B. *Chemistry in Motion. Reaction-Diffusion Systems for Micro- and Nanotechnology,* 1st ed.; John Wiley & Sons: West Sussex, **2009**.

(3) Hwang, I.; Mukhopadhyay, R. D.; Dhasaiyan, P.; Choi, S.; Kim, S.-Y.; Ko, Y. H.; Baek, K.; Kim, K. Audible Sound-Controlled Spatiotemporal Patterns in out-of-Equilibrium Systems. *Nat. Chem*. **2020**, *12*, 808–813.

(4) Lengyel,I.; Epstein, I. R. A Chemical Approach to Designing Turing Patterns in Reaction- Diffusion Systems. *PNAS* **1992**, *89*, 3977- 3979.

(5) Liesegang, R., E. Ueber Einige Eigenschaften von Gallerten. *Naturwiss. Wochenschr* **1896**, *30*, 353-362.

(6) Ezzeddine, D.; El-Rassu, H.; Sultan, R. Surface and Structural Studies in a $PbCrO_4$ Liesegang Pattern with Revert Spacing. *Chem. Phys. Lett*. **2019**, *734*, 136735.

(7) Smoukov, S. K.; Lagzi, I.; Grzybowski, B. A. Independence of Primary and Secondary Structures in Periodic Precipitation Patterns. *J. Phys. Chem. Lett*. **2011**, *2*, 345-349.

(8) Krug, H-J.; Brandtstadter, H. Morphological Characteristics of Liesegang Rings and Their Simulations. *J. Phys. Chem*. A **1999**, *103*, 7811- 7820.

(9) Xie, D.; Wu, J.; Xu, G.; Ouyang, Q.; Soloway, R.D.; Hu, T. Three-Dimensional Periodic and Fractal Precipitation in Metal Ion- Deoxychalate System: A Model for Gallstone Formation. *J. Phys. Chem*. A **1999,** *103*, 8602- 8605.

(10) Thomas, S.; Lagzi, I.; Molnár, F.; Rácz, Z. Helices in the Wake of Precipitation Fronts. *Phys. Rev. E* **2013**, *88*, 022141.

(11) Nabika, H.; Itatani, M.; Lagzi, I. Pattern Formation in Precipitation Reactions: The Liesegang Phenomenon. *Langmuir* **2020**, *36*, 481–497.

(12) Zhang, H.; Zhan, K.; Chen, Y.; Chen, G.; Zhou, X.; Liu, J.; Wu, M.; Ni, H. Three Dimension Liesegang Rings of Calcium Hydrophosphate in Gelatin. *J Solgel Sci Techno* **2014**, *71*, 597–605.

(13) Bensemann, I. T.; Fialkowski, M.; Grzybowski, B. A. Wet Stamping of Microscale Periodic Precipitation Patterns. *J. Phys. Chem. B* **2005**, *109*, 2774–2778.

(14) Farkas, S.; Holló, G.; Schuszter, G.; Deák, Á.; Janovák, L.; Hornok, V.; Itatani, M.; Nabika, H.; Horváth, D.; Tóth, Á.; Lagzi, I. Reaction–Diffusion Assisted Synthesis of Gold Nanoparticles: Route from the Spherical Nano-Sized Particles to Micrometer-Sized Plates. *J. Phys. Chem. C* **2021**, *125*, 26116–26124.

(15) Chopard, B.; Luthi, P.; Droz, M. Microscopic Approach to the Formation of Liesegang Patterns. *J. Stat. Phys*. **1994**, *76*, 661–677.

(16) Tasaki, S.; Nakayama, M.; Shoji, W. Morphologies of Bacillus Subtilis Communities Responding to Environmental Variation. *Dev. Growth Differ*. 2017, *59*, 369–378

(17) Nakahara, A.; Shimada, Y.; Wakita, J.; Matsushita, M.; Matsuyama, T. Morphological Diversity of the Colony Produced by Bacteria *Proteus Mirabilis .JPSJ* **1996**, *65*, 2700–2706

(18) Joseph, E.; Cario, S.; Simon, A.; Wörle, M.; Mazzeo, R.; Junier, P.; Job, D. Protection of Metal Artifacts with the Formation of Metal–Oxalates Complexes by Beauveria Bassiana. *Front. Microbiol*. **2012**, *2*.

(19) Gavin, K.; Banville, N. ; Gibbons, D.; Quinn, C. Liesegang rings in inflammatory breast lesions. *J. Clinic. Pathol*. **2006**, *58*, 1343- 1344.

(20) D. Demezhko. “Liesegang Rings” Imaggeo. Accessed: 10 March 2023. [Online]. Available: https://imaggeo.egu.eu/view/1948/

(21) Xing, Z.; Zhang, G.; Ye, J.; Zhou, Z.; Gao, J.; Du, B.; Yue, K.; Wang, Q.; Liu, J. Liesegang Phenomenon of Liquid Metals on Au Film. *Adv. Mater*. **2022**, *35*, 2209392.

(22) Kanniah, N.; Gnanam, F. D; Ramasamy, P. A New Spacing Law for Liesegang Rings. *Proc. Indian Acad. Sci.: Chem. Sci.* **1984**, *93*, 801–811.

(23) Itatani, M.; Fang, Q.; Nabika, H. Modification of the Matalon–Packter Law for Self-Organized Periodic Precipitation Patterns by Incorporating Time-Dependent Diffusion Flux. *J. Phys. Chem. B* **2021**, *125*, 6921–6929.

(24) Kulkarni, S. D.; Walimbe, P. C.; Ingulkar, R. B.; Lahase, J. D.; Kulkarni, P. S. Revert Banding in One-Dimensional Periodic Precipitation of the (AgNO3 + KBr) System in Agar Gel. *ACS Omega* **2019**, *4*, 13061–.13068.

(25) Karam, T.; El-Rassy, H.; Sultan, R. Mechanism of revert spacing in a $PbCrO_4$ Liesegang System. *J. Phys. Chem. A* **2011**, *115*, 2994-2998.

(26) Kanniah, N.; Gnanam, F.; Ramasamy, P.; Laddha, G. Revert and direct type Liesegang phenomenon of silver iodide. *J. Colloid Interface Sci*. **1981**, *80*, 369-376.

(27) Venzl, G. Patten Formation in Precipitation Processes. II. a post nucleation theory of Liesegang Bands. *J. Chem. Phys*. **1986**, *85*, 2006-2011.

(28) Hayashi, H.; Aoki, S.; Abe, H. Magnetic-Field-Induced Painting-Out of Precipitation Bands of Mn-Fe-Based Prussian Blue Analogues in Water-Glass Gels. *ACS Omega* **2018**, *3*, 4494–4501

(29) Lagzi, I. Formation of Liesegang Patterns in an Electric Field. *Phys. Chem. Chem. Phys*. **2002**, *4*, 1268- 1270.

(30) Khan, M. T. A.; Kwiczak-Yiğitbaşl, J.; Tootoonchian, P.; Morsali, M.; Lagzi, I.; Baytekin, B. Chemical Tracking of Temperature by Concurrent Periodic Precipitation Pattern Formation in Polyacrylamide Gels. *ACS Appl. Mater. Interfaces* **2022**, *14*, 7252–7260.

(31)Ambrose, S.; Gnanam, F. D.; Ramasamy, P. Periodic Crystallisation of Magnesium Hydroxide in Agar-Agar Gel. Influence of Temperature. *Proc. Indian Acad. Sci. (Chem. Sci.)* **1983**, *92*, 239-247.

(32) Prakash, S. M. D.; Rao, P. M. Periodic Crystallization of Barium Oxalate in Silica Hydrogel. *Bull. Mater. Sci*. **1986**, *8*, 511–517

(33) Morsali, M.; Khan, M. T. A.; Ashirov, R.; Holló, G.; Baytekin, H. T.; Lagzi, I.; Baytekin, B. Mechanical Control of Periodic Precipitation in Stretchable Gels to Retrieve Information on Elastic Deformation and for the Complex Patterning of Matter. *Adv. Mater.* **2020**, *32*, 1905799.

(34) García-Ruiz, J. M.; Rondón, D.; García-Romero, A.; Otálora, F. Role of Gravity in the Formation of Liesegang Patterns. *J. Phys. Chem*. **1996**, *100*, 8854–8860.

(35) Swami, S. N.; Kant, K. Effect of Light on the Formation of Liesegang Rings of Copper Chromate in Agar Agar Gel. *Colloid Polym Sci.* **1967**, *215*, 60–61.

(36) Rajurkar, N.; Ambekar, B. Studies on Liesegang Rings of Cobalt Hydroxide in 1% Agar Gel Medium. *J Mol Liq.* **2015**, *204*, 205–209.

(37) Shreif, Z.; Mandalian, L.; Abi-Haydar, A.; Sultan, R. Taming Ring Morphology in 2D Co(OH)2 Liesegang Patterns. *Phys. Chem. Chem. Phys.* **2004**, *6*, 3461–3466.

(38) Holló, G.; Zámbó, D.; Deák, A.; Rossi, F.; Cucciniello, R.; lo Nostro, P.; Nabika, H.; Baytekin, B.; Lagzi, I.; Itatani, M. Effect of the Polarity of Solvents on Periodic Precipitation: Formation of Hierarchical Revert Liesegang Patterns. *J. Phys. Chem. B* **2022**, *126*, 8322–8330.

(39) Ibrahim, H.; El-Rassy, H.; Sultan, R. Liesegang Bands versus Random Crystallites in Ag2Cr2O7 – Single and Mixed Gelled Media. Chem. Phys. Lett. **2018**, *693*, 198–201.

(40) Shreif, Z.; Mandalian, L.; Abi-Haydar, A.; Sultan, R. Taming Ring Morphology in 2D Co(OH)2 Liesegang Patterns. Phys. Chem. Chem. Phys. **2004**, *6*, 3461.

(41) M. Fialkowski, A. Bitner and B. A. Grzybowski, Wave Optics of Liesegang Rings, Phys. Rev. Lett. **2005**, *94*, 083183.

(42) Akbulut, E. S.; Hollo, G.; Lagzi, I., Baytekin B. **2023**, submitted.

(43) Thomas, S.; Molnár, F.; Rácz, Z.; Lagzi, I. Matalon-Packter Law for Stretched Helicoids Formed in Precipitation Processes. *Chem Phys Lett.* **2013***, 577,* 38–41.

(44) Spreadborough, J.; Christian, J. W. High-Temperature X-Ray Diffractometer. J. Sci. Instrum. **1959**, *36*, 116–118.

(45) Matsushita, M.; Wakita, J.; Itoh, H.; Watanabe, K.; Arai, T.; Matsuyama, T.; Sakaguchi, H.; Mimura, M. Formation of Colony Patterns by a Bacterial Cell Population. *Phys. A: Stat*. **1999**, *274*, 190–199.

(46) Kovacs, A. T. Bacillus Subtillis. *Trends Microbiol.* **2019**, *27*, 724- 725

(47) Adelnia, H.; Ensandoost, R.; Shebbrin Moonshi, S.; Gavgani, J. N.; Vasafi, E. I.; Ta, H. T. Freeze/Thawed Polyvinyl Alcohol Hydrogels: Present, Past and Future. *Eur. Polym. J.* **2022**, *164*, 110974.

(48) Fujikawa, H. Diversity of the growth patterns of Bacillus subtilis colonies on agar plates. *FEMS Microbiol. Ecol.* **1994**, *13*, 159-167.

(49) Salem, M.; Mauguen, Y.; Prange, T. Revisiting glutaraldehyde cross-linking: the case of the Arg-Lys intermolecular doublet. *Acta Crystallogr. F:Struct. Biol.* **2010**, *66*, 225-228.

(49) Adelnia, H.; Ensandoost, R.; Shebbrin Moonshi, S.; Gavgani, J. N.; Vasafi, E. I.; Ta, H. T. Freeze/Thawed Polyvinyl Alcohol Hydrogels: Present, Past and Future. *Eur. Polym. J*. **2022**, *164*, 110974.

(50) Song, X.; Sun, S.; Zhang, D.; Wang, J.; Yu, J. Synthesis and Characterization of Magnesium Hydroxide by Batch Reaction Crystallization. *Front Chem Sci Eng*, **2011**, *5*, 416–421.

(51) Petrucci, H. R.; Herring, G. F.; Bissonnette, C.; Madura, J. D. *General Chemistry: Principles and Modern Applications;* Pearson Education, **2017**.

(52) Pannach, M.; Bette, S.; Freyer, D. Solubility Equilibria in the System Mg(OH)2–MgCl2–H2O from 298 to 393 K. *J. Chem. Eng. Data* , **2017,** *62*, 1384–1396.

(53) Sierra-Fernandez, A.; Gomez-Villalba, L. S.; Milosevic, O.; Fort, R.; Rabanal, M. E. Synthesis and Morpho-Structural Characterization of Nanostructured Magnesium Hydroxide Obtained by a Hydrothermal Method. *Ceram. Int.* **2014**, *40*, 12285–12292.

(54) Henrist, C.; Mathieu, J.-P.; Vogels, C.; Rulmont, A.; Cloots, R. Morphological Study of Magnesium Hydroxide Nanoparticles Precipitated in Dilute Aqueous Solution. J. Cryst. Growth **2003**, *249*, 321–330.

(55) Tai, C. Y.; Tai, C.-T.; Chang, M.-H.; Liu, H.-S. Synthesis of Magnesium Hydroxide and Oxide Nanoparticles Using a Spinning Disk Reactor. *Ind. Eng. Chem. Res.* **2007**, *46*, 5536–5541.

(56) Chakoumakos B.C.; Horita J.; Garlea V.O. H/D isotope effects in brucite at low temperatures : At 20 K. *Am Min.* **2013**, *98*, 1-6.

(57) Stellwagen, N. C. Electrophoresis of DNA in Agarose Gels, Polyacrylamide Gels and in Free Solution. Electrophor. **2009**, *30*, S188–S195.

(58) Løge, I. A.; Anabaraonye, B. U.; Bovet, N.; Fosbøl, P. L. Crystal Nucleation and Growth: Supersaturation and Crystal Resilience Determine Stickability. Cryst. Growth Des. Design, **2023**, *23*, 2619–2627.

(59) Ge, J. C.; Wu, G.; Yoon, S. K.; Kim, M. S.; Choi, N. J. Study on the Preparation and Lipophilic Properties of Polyvinyl Alcohol (PVA) Nanofiber Membranes via Green Electrospinning. Nanomater., **2021**, *11*, 2514.